This is to certify that the

thesis entitled

Colin Gregor MacKinnon

presented by

INFLUENCE OF FORCING ON THE COMPOSITION OF MIXED FLUID
IN A TWO-STREAM SHEAR LAYER

has been accepted towards fulfillment
of the requirements for

Masters degree in Mechanical Engineering

M. M. Koochesfahani

Major professor

Date May 10, 1991

INFLUENCE OF FORCING ON THE COMPOSITION OF MIXED FLUID IN A TWO-STREAM SHEAR LAYER

By

Colin Gregor MacKinnon

A THESIS

Submitted to
Michigan State University
in partial fulfillment of the requirements
for the degree of

MASTER OF SCIENCE

Department of Mechanical Engineering

1991

ABSTRACT

INFLUENCE OF FORCING ON THE COMPOSITION OF MIXED FLUID IN A TWO-STREAM SHEAR LAYER

By

Colin Gregor MacKinnon

Experiments are conducted in a non-reacting forced liquid shear layer. The probability density function (pdf) of mixed-fluid composition is measured using laser induced fluorescence diagnostics. Results show that the range of compositions of mixed fluid in forced layers is essentially uniform across the width of the shear layer, similar to previous results in natural (unforced) shear layers. We also found that forcing leads to an increase in the total amount of mixed fluid (integrated across the layer) and that the predominant mixed-fluid concentration shifts to larger values. This increase in the amount of mixing appears to be mostly due to the increased width of the layer and not so much the result of improved small-scale mixing. In addition, the details of the forcing waveform shape (frequency content) are observed to have a significant effect on the structure of the flow and the mixing field.

Dedicated to the memory of my mother,

Margaret L. MacKinnon

ACKNOWLEDGEMENTS

I am indebted to my advisor Dr. Manooch Koochesfahani for his advice, support and, above all, patience throughout the pursuit of this degree. This research was sponsored by AFOSR Contract Nos. AFOSR-87-0332 and AFOSR-89-0130

TABLE OF CONTENTS

LIST OF TABLES

LIST OF FIGURES

LIST OF SYMBOLS

Symbol	Description
C_{2_0}	low-speed freestream reactant (molar) concentration
C_d	dye concentration
C_{d_0}	low-speed freestream dye concentration
$\overline{c_p}(y)$	average product concentration
E	entrainment ratio
F	forcing frequency
$F(t)$	forcing waveform
h	test-section half-width
I	fluorescence intensity
I_0	(corrected) low-speed freestream fluorescence intensity
I_{backg}	background fluorescence intensity
I_{corr}	corrected fluorescence intensity
M	molar concentration
$p(\xi,y$	pdf of ξ at y
$p_0(y)$	probability of finding pure low-speed fluid at y
$p_1(y)$	probability of finding pure high-speed fluid at y
$p_m(y)$	probability of finding mixed fluid at y
$P(\xi)$	averaged pdf of ξ
r	velocity ratio, U_1/U_2
R	growth rate parameter, $(U_1-U_2)/(U_1+U_2)$
Re_{δ_1}	Reynolds number, $\Delta U \delta_1/\nu$
S	symmetry parameter of forcing waveform
U	mean velocity
U_1	high-speed freestream velocity

U_2	low-speed freestream velocity
U_c	convection speed of large structures
υ_1	volume of high-speed fluid in the sampling volume
υ_2	volume of low-speed fluid in the sampling volume
x	downstream distance
X_{WO}	Wygnanski-Oster parameter, RxF/U_c
δ_1	shear layer 1% thickness
δ_m	mixed-fluid thickness
δ_ω	vorticity thickness
δ_{p_1}	product thickness
δ_{p_2}	product thickness
δ_{vis}	shear layer viual thickness
ε	small number
θ_0	initial layer momentum thickness
θ	layer momentum thickness
λ_D	smallest scalar diffusion scale
λ_K	Kolmogorov scale
ν	kinematic viscosity
ξ	high-speed fluid volume fraction
pdf	probability density function
LIF	laser induced fluorescence

Chapter 1

INTRODUCTION

The present work is concerned with a special case of plane shear flows. This group of flows is mainly composed of 2D wakes, 2D jets and plane shear layers. In particular, we will be dealing with a homogeneous plane free shear layer. This type of flow arises when two fluids of different speeds, which are initially separated by a thin partition (for example, a splitter plate), merge with each other. In our study we have used water in both streams. Thus the density is the same on both sides of the layer, although in general this is not the case. The use of the word 'free' refers to the fact that the flow is not influenced by the presence of any boundaries beyond the trailing edge of the partition. A schematic of the flow configuration is shown in Figure 1.

If the Reynolds number is high enough, intense mixing occurs in the region of the velocity gradient between the streams. For this reason such shear layers are often called mixing layers. The dramatic increase in the amount of mixing as the Reynolds number is increased was called the *mixing transition* by Konrad (1976). This will be discussed in more detail later in the introduction.

Over the past few decades shear layers have been the subject of a great deal of attention. Part of the reason for this attention is that shear layers, and, in particular, turbulent shear layers, appear in a vast number of naturally-occurring flows, flows in engineering applications and industrial flows. Examples of naturally-occurring shear layers are abundant. A simple example is that of the wind blowing over the surface of an ocean, creating surface waves. On the practical side, shear layers occur - amongst other places - in combustors, chemical lasers and in the separated region of the flow over an airfoil. A second motivation for the interest in mixing layers is that they are generally regarded as one of the simplest turbulent shear flows. Consequently, the effects of velocity ratio, density ratio etc., have been relatively easy to investigate in the laboratory. Results from the study of shear layers have played an important role in developing the modern view of turbulent shear flows (see, for example, the review by Roshko (1976)).

1.1 Background

There have been many significant experimental works related to the present study in recent years. These studies fall into three main categories which will be discussed in turn in the following paragraphs.

The Natural Layer

A shear layer which is not subjected to any intentionally imposed disturbances is called a *natural* shear layer. Probably the most important discovery in this area was made by Brown & Roshko (1971, 1974). They initially wanted to study the effect of a density difference on their gaseous layer. However, they were astonished to find that the flow was dominated by large coherent structures over a wide range of Reynolds numbers. Their shadowgraph pictures also showed that a fine mesh of small scale three-dimensional motions was superposed on the background of the large structures.

At about the same time, Winant & Browand (1974) proposed that the main mechanism by which the shear layer grows is by the amalgamation of two neighboring structures into a single larger structure. They called this interaction 'pairing'. In the natural layer the vortices are irregularly spaced so that when pairings take place, the growth rate of the layer increases, on the average, in a linear fashion.

The work of Dimotakis & Brown (1976) showed that the large scale motions persisted, in a liquid mixing layer, up to Reynolds numbers of 3×10^6. This Reynolds number was based on the velocity of the high-speed stream and the distance from the trailing edge of the splitter plate to the measurement location. They also pointed out that the dynamics of the shear layer may in fact be governed by a global 'feedback mechanism'.

The formation and persistence of the organised two-dimensional structures has been documented in numerous other investigations (for example, Rebollo (1973), Browand & Weidman (1976), Wygnanski *et al.* (1979B), Browand & Ho (1983)). There is, however, a secondary structure present in the flow. Miksad (1972) observed weak longitudinal vortex structures in his gaseous layer, and concluded that 'once a secondary vortex structure is established transition to turbulence occurs'. In the works of Konrad (1976) and Breidenthal (1978, 1981), plan views of their shear layers revealed streamwise streaks. Breidenthal interpreted these to be pairs of streamwise vortices of alternating signs. This was confirmed by the (y-z) cross-sectional views of Bernal (1981). His pictures showed structures composed of pairs of counter-rotating streamwise vortices superimposed on the spanwise vortices. Lasheras, Cho & Maxworthy (1986) and Lasheras & Choi (1988) have made recent investigations (using three-dimesional forcing) into the origins of the streamwise structures. They concluded that perturbations in the spanwise vorticity, subjected to a large straining field between the primary vortices, are stretched in the axial direction resulting in pairs of counter-rotating streamwise vortices. Nygaard & Glezer (1991) have studied the interactions of the spanwise and streamwise vortices and proposed a method by which these interactions lead to the generation of small scale three-dimensional motions. The production of small scale motion is generally believed to be the mechanism which increases mixing in the layer, by means of increased interfacial area (Jìmenez, Martinez-Val & Rebollo (1979)).

Thus, a simplified view of the development of the flow in a turbulent shear layer is given by the following. It is well known that for a shear layer with laminar boundary layers on the splitter plate, disturbances are amplified immediately downstream of the plate by Kelvin-Helmholtz instability. These disturbances grow from the plate tip with a certain natural frequency which is dependent on the velocity ratio and the initial momentum thickness, θ_0, of the layer. These instability waves initially grow exponentially until the large spanwise structures have developed. Through the interaction of these structures with the streamise vortices small-scale motions are produced, which subsequently leads to enhanced mixing within the layer. Just prior to the establishment of fully rolled-up vortices the flow can satisfactorily be described by linear inviscid stability theory (Michalke (1965)). The ensuing interactions of the primary and secondary vortices resulting in the fine scale three-dimensional motions need further investigation to enable a more complete understanding.

Mixing

The vast majority of research in shear layers, and shear flows in general, has concentrated on the momentum transport properties of the flow. Quantities typically measured include mean and rms velocities, frequency spectra of the velocity fluctuations, Reynolds stresses and, more recently, vorticity (Lang (1985), Foss & Haw (1990), Foss & Wallace (1989), Ballint *et al.* (1988)). Studies concerned with the actual extent of the *mixing*, by contrast, have been far fewer.

Some notable exceptions are the works of Konrad (1976), Breidenthal (1978, 1981) and Koochesfahani (1984, 1986). Konrad used a concentration sampling probe in a non-reacting gaseous layer to infer the amount of mixing, whereas Breidenthal used an absorption technique in a chemically reacting liquid layer to deduce the amount of chemical product. They found that a rapid increase in the amount of mixing (or chemical product) occurred some distance downstream of the splitter plate (or, equivalently, when the Reynolds number became sufficiently large). The increase in mixing was attributed to the increase of interfacial area between the two fluids, which, in turn, was a consequence of the development of small-scale three-dimensional motions. In Figure 2 a plot is reproduced from Roshko (1990) which describes the mixing transition. A measure of the mixedness is plotted against large structure Reynolds number $\Delta U \delta_\omega / \nu$, where $\Delta U = U_1 - U_2$, ν is the kinematic viscosity, and δ_ω is the vorticity thickness, given by $\Delta U / (\partial U / \partial y)_{max}$, where U is the mean velocity. The vorticity thickness is approximately ½ the 'visual thickness' of the shear layer.

A recent study by Huang & Ho (1990) has led to the conclusion that the small-scale motions are initiated by the interaction of *merging* spanwise vortices with streamwise vortices. The computational study of Moser & Rogers (1990) found that 'when the flow is sufficiently three-dimensional, a pairing can cause the mixing layer to undergo a transition to small-scale turbulence'. The mixing of a passive scalar was seen to increase with this small-scale transition. A more detailed account of the current views regarding the mixing transition may be found in Roshko (1990).

Koochesfahani (1984) introduced the technique of *laser-induced fluorescence* (LIF) both as a means to measure the extent of the molecular mixing and for excellent flow visualization. In his liquid layer, both chemically reacting and non-reacting (passive scalar mode) experiments were performed. The main results were that, during the mixing transition, the amount of mixed fluid increased and that, at the same time, the dominant mixed-fluid concentration changed. It was also found that the *range* of concentrations corresponding to significant mixed-fluid probabilities was essentially fixed across the entire transverse extent of the layer. Figure 15 shows this feature - the position of the 'hump' with respect to the ξ-axis remains almost constant as one crosses the layer in the y direction. This latter feature was also shown in Konrad's work. The LIF technique is used in the present study, although in the non-reacting mode.

The Forced Layer

For an excellent review of forced shear layer results the reader is referred to Ho & Huerre (1984).

Some of the earlier works in (pre-mixing transition) shear layers (Freymuth (1966), Browand (1966)) were undertaken in an attempt to establish a link between the instability of the flow and the onset of turbulence. However, the researchers found that there was a large amount of spatial 'jitter' in the flow. This was due to the fact that, in a natural layer, instability waves in a wide range of frequencies are amplified, even though there is a dominant natural frequency. The different phase-speeds of these waves then produced the irregularity which was observed. As a remedy for this situation, low-level forcing at about the natural frequency was applied to the layers. This provided a clear phase reference which allowed more stable measurements to be made. It was thought that there was no effect on the dynamics of the flow, other than a decrease in broadband noise.

It later became apparent (Oster & Wygnanski (1982), Ho & Huang (1982), Zaman & Hussain (1981)) that, in fact, external periodic oscillations at relatively low amplitudes can significantly affect the growth rate of the shear layer, and that the large structures can, to some extent, be controlled by them.

The dramatic effect of two-dimensional forcing on the layer growth rate is illustrated in Figure 3, which has been reproduced from the thesis of Roberts (1985). A representative segment for the growth rate of a natural layer has been included at the right hand side of this plot for comparison. The data for this plot were taken from the forced layers of Oster & Wygnanski and Ho & Huang and plotted on the same graph by Browand & Ho (1983). The data of Oster & Wygnanski was obtained from a high Reynolds number, post-mixing-transition layer, while that of Ho & Huang was produced mainly in pre-mixing-transition experiments. From this figure it can be seen that, instead of the linear growth found in natural layers, the forced layer experiences three different types of growth. Initially the growth rate is enhanced, compared to the natural case. Then there is a period of little or no growth, and finally the growth approaches that of the natural layer.

This plot shows the normalized growth rate as a function of the Wygnanski-Oster parameter, first introduced in Oster & Wygnanski (1982), and given by,

$$X_{WO} = \frac{RxF}{U_c}. \tag{1.1}$$

This dimensionless parameter encompasses the effects of the ratio, $R = (U_1 - U_2)/(U_1 + U_2)$, to which the post-mixing-transition growth rates are proportional, the forcing frequency, F, and the downstream distance, x. U_c is the convection speed of the vortical structures, given by $U_c \approx \frac{1}{2}(U_1+U_2)$ for a uniform density shear layer. The growth of the layer is measured by the momentum thickness, θ, given by,

$$\theta = \int_{-\infty}^{\infty} \frac{(U_1-U)(U-U_2)}{(U_1-U_2)^2} dy, \tag{1.2}$$

which, in the plot, has been normalized by U_c/F.

Oster & Wygnanski found that they could segregate the flow into three main parts, representing the different response characteristics mentioned above. These regions of the flow were categorized in the following way :

I $X_{WO} < 1$: the growth rate is enhanced by a factor of 2 or more,

II $1 < X_{WO} < 2$: the flow forms a periodic array of vortices with passage frequency equal to the forcing frequency; the growth rate is inhibited in this 'frequency-locked' region, even reduced to zero; Reynolds stresses are reversed in sign,

III $X_{WO} > 2$: relaxation to unforced growth rate.

It should be noted, as in Roberts (1985), that, although both post- and pre-mixing transition data fall quite well onto this plot, it should not be regarded as a 'universal' curve. In fact, Ho & Huerre (1984) show a similar plot with a great deal more 'scatter' in the data.

Ho & Huang (1982) showed how they could manipulate the growth rate and control vortex merging by forcing the layer at a subharmonic of the most-amplified (or natural) frequency. For example, forcing the layer at the first subharmonic produced pairing of neighboring vortices and forcing at the second subharmonic yielded 'tripling'. They also found that pairing took place at the downstream location where the energy of the subharmonic mode of the velocity fluctuation reached its peak. This illustrated the importance of the development of the subharmonic mode of the shear layer to the process of vortex merging.

The forced studies cited above have all been concerned with the effects of *two-dimensional* forcing on various aspects of the shear layer. However, three-dimensional forcing is becoming a most useful tool in trying to understand the complexities of this flow. Breidenthal (1980) was one of the first to perform such a study on shear layers and wakes, and currently Lasheras, Cho & Maxworthy (1986), Lasheras & Choi (1988) and Nygaard & Glezer (1991), among others, are making advances with this approach.

1.2 Objective

In all of these forced layer studies, with the exception of Roberts (1985), there has been no emphasis on the actual mixing. The purpose of the present work is to attempt to shed some light on this topic by answering the question : 'how does two-dimensional forcing affect the actual species mixing in a shear layer ?'.

To the best of the author's knowledge the work of Roberts is the only experimental investigation giving information about the extent of the mixing in a two-dimensionally forced shear layer. Roberts made product concentration measurements in a reacting shear layer, using an absoption technique. His main findings were that, at high Reynolds numbers, external forcing reduced the amount of reaction product and that, at low Reynolds numbers, the amount of product increased, although there is some uncertainty in the latter result. The present study may be viewed as a further investigation of this problem. There are, however, two main differences between these works. Firstly, Roberts used a chemically reacting shear layer, while we have used a non-reacting layer. Secondly, Roberts obtained product concentration measurements integrated through the layer, due to the nature of his absorption technique, whereas the present method provides (passive scalar) concentration information at any point across the layer.

Chapter 2

EXPERIMENTAL FACILITY AND INSTRUMENTATION

The data for this study were acquired during a single set of experiments, one experiment for each of five forcing conditions. In this chapter the equipment used and the data acquisition and reduction processes are described.

2.1 Shear Layer Facility

The experiments were performed in a gravity driven liquid shear layer apparatus, a schematic of which is shown in Figure 4. The majority of the facility was fabricated in house by Mr. R. Schrader. The working fluid in both streams was water.

Water was pumped from each of the two independent reservoirs up to the overhead tanks, where, in each, a constant head was maintained by making use of an overflow chamber. In addition, a constant head was maintained at the outlet of the test section. These measures minimized fluctuations of the free-stream speeds which may have arisen as a result of time dependent boundary conditions at the inflow and outflow. The flow rates were controlled by three valves, one in each supply line upstream of the test section, and one downstream of the test section.

During the filling process, in preparation for an experiment, care was taken to expel as much air as possible from the contraction and flow management sections, since it was observed during some preliminary runs that the periodic surging of air bubbles could significantly affect the rms velocity levels in the layer.

The test section had a cross-section of 4 cm (height) x 8 cm (span) and was 35 cm long. The upper stream was arbitrarily chosen to be the high speed stream.

All of the statistical results in this study were obtained using free-stream speeds of U_1 = 40 cm/s and U_2 = 20 cm/s. This gave a velocity ratio of $r = U_2/U_1 = 0.5$. At these speeds, the Kelvin-Helmholtz instability produced a natural roll-up frequency of about 27 Hz. This figure was estimated by extrapolating from the data of a sequence of natural frequencies calculated from runs at lower speeds. The natural frequencies were obtained by counting the peaks in the velocity signatures from laser-Doppler measurements made just downstream of the trailing edge of the splitter plate.

2.2 Forcing Mechanism

Velocity perturbations have been introduced into shear layers, in the past, by many different techniques. For example, Oster & Wygnanski (1982) attached an oscillating flap at the trailing edge of the splitter plate. Ho & Huang (1982) used rotating valves in the test section supply lines. Acoustic excitation through loudspeakers has also been used frequently. In the present case, forcing was applied by means of an oscillating bellows operating in the high speed supply line, near the entrance to the contraction. A schematic of the bellows mechanism is shown in Figure 5. The motion was controlled by a magnetic coil vibrator and amplifier system (VTS 50), the input to which was supplied by a function generator (HP3314A).

The experimental runs conducted for this study were different from each other only with respect to the parameters of the forcing waveform used. In one case there was no forcing, i.e. the natural shear layer resulted. For the next two cases sinusoidal forcing of frequencies 4 Hz and 8 Hz, respectively, was used. To investigate the effects of non-sinusoidal forcing, the symmetry, S, of the 4 Hz waveform was varied which provided skewed sine wave motions.

The symmetry of a waveform, as far as our experiments are concerned, is the percentage of one period of the motion that the bellows spends moving downwards. Figure 6 illustrates the effect of varying the symmetry of a sine wave. A sine wave spends the same amount of time increasing as it does decreasing and therefore has a symmetry value of $S = 50\%$. A symmetry value $S = 70\%$ indicates that the bellows spends 70% of its period moving downwards. In this case, the bellows moves down slowly and goes up quickly. Perhaps a better way to view this is that the free-stream speed increases slowly and decreases quickly. The non-sinusoidal waveforms used had 4 cycles per second and symmetry values of $S = 30\%$ and $S = 70\%$, respectively.

It is important to note that a symmetry value other than 50% indicates that the waveform has more than one frequency component. This fact will be used in Chapter 3 in an attempt to explain an interesting observation.

2.3 Diagnostics

Quantitative concentration information was obtained using the technique of laser induced fluorescence (LIF). A brief description of this method is given below; for a complete account the reader is referred to Koochesfahani & Dimotakis (1985).

For this technique it is necessary that one of the free-streams carries a fluorescent dye. In our case, the low-speed stream was prepared by adding a solution of disodium fluorescein dye and the high-speed stream was pure water. The dye solution was thoroughly premixed with the water in the low-speed reservoir to a concentration of approximately 5×10^{-7} M (molar concentration). This initial concentration, C_{d_0}, becomes diluted as the pure fluid from the high-speed stream mixes with the low-speed stream in the shear layer.

The local instantaneous concentration of the dye, C_d, in a sampling volume is given by

$$C_d = C_{d_0} \frac{\upsilon_2}{\upsilon_1 + \upsilon_2}, \tag{2.1}$$

where υ_1 is the volume of high speed fluid and υ_2 is the volume of low speed fluid within the sampling volume. A normalized concentration, ξ, can then be defined as

$$\xi = 1 - C_d / C_{d_0}, \tag{2.2}$$

which is simply the high-speed fluid volume fraction, $\upsilon_1/(\upsilon_1 + \upsilon_2)$. Note that values of $\xi = 0$ and $\xi = 1$ correspond to pure low-speed fluid and pure high-speed fluid, respectively. Values of concentration in the range $0 < \xi < 1$ indicate mixed fluid.

The shear layer concentration data were acquired over a downstream region 15 cm $\leq x \leq$ 25 cm. The Reynolds number in the middle of this range was about $Re_{\delta_1} = 6600$. This Reynolds number was based on the layer width, δ_1, (see appendix) and the velocity difference, $\Delta U = U_1 - U_2$. This corresponds to a shear layer in the latter stages of the mixing transition (Breidenthal (1981)). We note that we would have preferred to realize a higher Reynolds number. Unfortunately, we were limited by the flow speeds available and the dimensions of the test-section. In fact, Figure 12 shows that the growth of the structures could be inhibited by the width of the test-section. This prevented us from moving to an imaging location further downstream where we would have achieved a higher Reynolds number.

The beam from a 4 watt argon-ion laser (Excel 3000) was focused through a converging lens and then passed through a cylindrical lens to produce a thin (about 1 mm in thickness) laser sheet. This sheet was aligned vertically with the transverse direction and horizontally with the streamwise direction at the midspan position of the test section. Figure 7 shows a schematic of this set-up.

The fluorescence intensity resulting in the shear layer was proportional to the local dye concentration and to the local laser intensity. These intensities were then recorded by a 2-D CCD video camera (NEC TI-24A), which was operating at 60 fields/s with an exposure time of 2 msec. This camera contains a 2-D array of 512 x 480 "pixels" which converted the incoming light intensities to voltages. In our experiments, the 4 cm width of the test section was imaged onto 200 pixels which resulted in a spatial resolution of 200 μm x 200 μm. The 512 horizontal pixels then enabled measurements over a 10 cm streamwise range.

The signal from the camera was, in turn, digitized to 8 bits and stored on hard disk in real time by a digital image acquisition system (Trapix 5500). Typically, 256 sequential images (64 MBytes of data) were acquired for each run. This volume of data was considered sufficient for the present purpose. The 2-D images allowed the development of the concentration field to be monitored in two dimensions. For the 4 Hz cases the data corresponded to the passage of about 34 large structures and to about 68 structures for the 8 Hz case.

The LIF technique has an important limitation when used in the passive scalar mode (Koochesfahani (1984)). This technique always overestimates the amount of mixed fluid (i.e. it provides an upper bound to the actual molecular mixing). The difficulty arises when the sampling volume of the measurement apparatus is larger than the smallest mixing scales, as is usually the case. It is then impossible to determine, within the resolution of the measuring device, whether or not two fluids are mixed. In the present study the camera recorded the region of the flow between 15 cm $\leq x \leq$ 25 cm. In the middle of this region (i.e. at x = 20 cm), the local natural shear layer width, δ_1 (see Appendix), was estimated to be about 3.3 cm, resulting in a local Reynolds number of 6600. Miller & Dimotakis (1991) have recently found results which indicate that the smallest expected scalar diffusion scale, λ_D, is very similar to the Kolmogorov scale, λ_K, in water. Using the Kolmogorov scale, taken as $\lambda_K = \delta_1 \mathrm{Re}^{-\frac{3}{4}}$, to estimate the smallest diffusion scale results in $\lambda_D \simeq 45\ \mu\mathrm{m}$ (at x = 20 cm). This is about 4.4 times smaller than the present 200 µm spatial resolution scale. Consequently, when mixing results are discussed in this work, what is implied is mixing on a scale commensurate with or larger than 200 µm. In spite this, it is felt that the changes found in the pdfs of the forced cases compared to the natural case reflect genuine trends, since the relative resolution (compared to the diffusion scale) is essentially the same in all of our measurements.

2.4 Data Reduction

The use of the LIF technique requires that the raw images be pre-processed before use by a histogram program. This process will now be described.

The laser sheet does not provide a uniform intensity. This is due to the Gaussian nature of the laser beam intensity distribution, the imaging optics and also the attenuation of the laser intensity due to absorption of energy by the dye molecules. This results in flow images which are deficient on two counts. Firstly the left and right edges have artificially low intensities. Secondly, two pixels corresponding to locations where the dye concentration is the same, one near the top of the test-section and one near the bottom, will have different intensities. A third feature of the system is that the individual camera pixels may have different response characteristics. We note that attenuation effects in the present experiments were negligible. The other discrepancies were all corrected by a simple method.

Immediately prior to the experimental runs, the test-section was completely filled with the dye solution from the low-speed freestream. This provided a reference or background intensity distribution which was recorded. The effects of the non-uniform laser sheet intensity were removed using the following calculation at each pixel :

$$I_{corr}(i,j) = \frac{I(i,j)}{I_{backg}(i,j)}, \quad i = 1, 512 \ , \ j = 1, 200 \ , \tag{2.3}$$

where $I(i,j)$ is the measured fluorescence intensity from the pixel in the i^{th} column and j^{th} row, $I_{backg}(i,j)$ is the background intensity and $I_{corr}(i,j)$ is the corrected intensity.

The actual concentration values (suppressing indices) were then obtained using

$$\xi = 1 - I_{corr} \,/\, I_0 \ , \tag{2.4}$$

where I_0 is the (corrected) intensity from the dye stream. Note that this is the same as equation (2.2), where we have used the fact that the fluorescence intensity is proportional to the local dye concentration and the local laser intensity.

The processed images were then passed to a histogram routine to create the various probability density functions.

Chapter 3

EXPERIMENTAL RESULTS

In this chapter qualitative visual and quantitative statistical results from the forced shear layer experiments are presented and discussed.

Preliminary runs were made to establish the quality of the flow near the entrance region to the test-section. Laser-Doppler measurements were taken of the streamwise velocity component at a location about $x = 1$ cm downstream from the splitter plate tip. Mean and rms velocity profiles from a typical run are displayed in Figure 8. The speeds used for this run were $U_1 = 14.4$ cm/s and $U_2 = 8.4$ cm/s. From the mean velocity profile in this figure it is apparent that each of the free-streams has a good degree of uniformity. Also shown is the typical "wake component" due to the boundary layers on either side of the splitter plate. This component evolves smoothly into the familiar 'tanh' profile with a sufficient downstream distance. The rms amplitude of the high-speed free-stream is about 0.6%. The double peak in the rms profile is also a result of the wake from the splitter plate. This feature, too, is smoothed out with downstream distance when it becomes a single broad peak with a large amplitude, signifying large velocity fluctuations in the middle of the layer.

Further runs were made to investigate the mean and rms velocities, at the same x-location, for the cases of the shear layer forced at frequencies of 1 Hz and 2 Hz. The results are shown in Figure 9. The natural frequency of this layer at the splitter plate tip was about 7 Hz. It was found that the mean velocity profiles for the forced cases deviated only slightly from the unforced profile even though the perturbation levels imposed on the flow were very high - the high speed free-stream peak-to-peak perturbation was about 14% of the mean speed. In fact, there are very few studies at such high forcing levels; however, this was the means of producing the 'collective interaction' process in the work of Ho & Huang (1982). The corresponding rms profiles, by contrast, showed very significant increases in velocity fluctuation compared to the unforced case.

All of the results discussed hereafter were obtained from experiments conducted with free-stream speeds $U_1 = 40$ cm/s and $U_2 = 20$ cm/s, giving a velocity ratio of $r = U_1/U_2 = 0.5$. The rms fluctuation imposed on the high-speed freestream was estimated to be less than 0.5%.

3.1 Visualization Results

Representative segments from sequences of 2D digital LIF images for each of the natural and forced cases are shown in Figures 10 - 13. Within each image the flow is from right to left and the high speed flow is on the top. Time is increasing downwards in each sequence. The content of each image is the concentration field of the mixing layer extending over the downstream region 15 cm $\leq x \leq$ 25 cm. The time between consecutive 'photographs' in each sequence is 1/15 second (a data rate of 60 fields per second is available from the camera). For the purposes of statistical analysis, a sequence typically consisting of 512 fields was acquired during each experiment. This corresponds to a total number of 34 structures in the 4 Hz case and 68 in the 8 Hz case.

The most readily observed feature is that noted previously by many experimenters - the forced layers show enhanced growth rates compared to the natural shear layer. In particular the 4 Hz, $S = 70\%$ case shows the largest increase in growth which we have observed so far. In fact, it is clear that the growth in this case is inhibited by the width of the test-section. By contrast, the 4 Hz, $S = 30\%$ case shows very little growth compared to the natural, and, indeed, resembles the natural layer to a surprising degree. This interesting observation will be addressed again later in the chapter. The pairing process, whereby two structures amalgamate into a single larger structure is also evident in these figures. The regions of the flow categorized by Oster & Wygnanski (1982) are also evident. Specifically, the 4 Hz cases ($X_{WO} = 0.9$) are in region I, characterized by pairing and enhanced growth rates. The 8 Hz case (X_{WO} = 1.8) is in the 'frequency-locked' state of region II. This case illustrates that the naturally most amplified frequency at this location is about 8 Hz.

In Figures 10 - 13 the concentration field is highlighted using various shades of grey, the general rule being 'darker greys mean higher concentrations of high speed fluid'. The range of ξ highlighted is $0.46 < \xi < 0.94$. Concentration levels outside of this range were present only in very small quantities and are therefore not labelled. The assignment of grey shades was linear.

The first observation that can be made is that, with the exception of the case F = 4 Hz & S = 30%, there is more mixing taking place in the forced layers than in the natural layer. This is apparent from the wider extent of grey shades seen within the structures of the forced cases. On closer inspection of these images it can be seen that the lighter greys which are predominant in the natural layer give way, in varying degrees, to darker greys in the forced cases. In other words, the predominant concentration shifts from relatively low values in the natural case to higher values for the forced cases. In fact, it will be shown by the data in the next section that this concentration increases progressively for each case in the following order : 8 Hz, 4 Hz, 4 Hz & S = 70%. A more dramatic display of the effects of forcing on the concentration field is shown in Figure 14. The image sequences shown are actually the same as in Figure 12 - namely the natural and 4 Hz, S = 70% cases - but they have a different grey shade assignment. The only concentrations that are highlighted are in the range $0.76 < \xi < 0.94$ and they are assigned to black. This emphasizes the shift in the predominant concentration to higher values for the forced case. These are the first indications that the mixing layer concentration field can be modified by external forcing.

From Figures 10 and 11 we can see that *single-frequency* forcing has a significant influence on the layer. A more surprising result is illustrated between Figures 12 and 13 - the cases of 4 Hz, S = 70% and 4 Hz, S = 30% respectively. The 70% case shows a much larger growth and indicates substantially more mixing. The forcing waveforms in these cases are composed of *more than one frequency*. From these we conclude that it is not merely the frequency of the forcing which affects the mixing but also the *shape* (or frequency content) of the forcing waveform. It may be argued that this effect is in fact the more dominant of the two.

All of the above observations are confirmed, in section 3.2, from a statistical view point, using the probability density function of the normalized concentration field for each of the cases.

3.2 Statistical Results

The focus of attention in this section is the probability density function of the high-speed fluid concentration, ξ. The pdf of ξ, at a given y-location, is denoted by $p(\xi,y)$ and it represents the fraction of time that $\xi(t)$ falls within a certain range of concentration values, $(\xi,\xi+\Delta\xi)$ for small $\Delta\xi$. This pdf is the basis for the definition of several other quantities of interest. The mathematical definitions of these quantities are given in the Appendix. The purpose of this section is to describe and interpret the results revealed by these quantities.

A typical pdf $p(\xi,y)$ exhibits two 'delta' functions at $\xi = 0$ and $\xi = 1$. These correspond to pure low and high speed fluid, respectively. In practice, these delta functions have a finite width, ε, dictated by the overall signal-to-noise ratio of the measurement. A value of ξ in the range $\varepsilon \le \xi \le 1-\varepsilon$ corresponds to mixed fluid. Pure low-speed fluid corresponds to the range $0 \le \xi < \varepsilon$ and the range $1-\varepsilon < \xi \le 1$ identifies pure high-speed fluid.

By collecting the information from pdfs at various y-locations across the width of the test-section we can construct contour plots of the concentration distributions for each of the forcing cases. Figure 15 shows the contour plot for the natural shear layer. The numerical values on the contours in this plot (and likewise for the forced cases) have been raised by a factor of 100 for simplicity. This plot displays the important result, documented previously by Koochesfahani (1984) for liquids in a natural layer, that the distribution of mixed-fluid concentration values is essentially uniform in the transverse direction of the layer.

When the layer is forced this uniformity is preserved, as can be seen from Figures 16 - 19. In fact, these plots lead us to the conclusion that the concentration distribution is 'even more' uniform upon external forcing. This may be expected from the following qualitative argument : since the larger vortices, created by forcing the layer, can redistribute and mix fluid from one side of the layer to the other more efficiently than in the natural layer, a more even distribution is achieved.

This property of shear layers allows us to integrate $p(\xi,y)$ in the y-direction to obtain an averaged pdf, denoted by $P(\xi)$. In this way a single pdf can represent the composition field of the whole layer.

Averaged pdf plots are shown in Figures 20 - 22. Figure 20 compares the natural case with the two sinusoidally forced cases (F = 4 and 8 Hz, S = 50%). Figure 21 compares the natural case with two of the 4 Hz cases, one forced sinusoidally and the other non-sinusoidally (F = 4 Hz, S = 50% and 70%). From these figures we can see two important features.

Firstly, when forcing is applied, the predominant concentration in each of the averaged pdfs shifts to larger values i.e. the peak concentration shifts to concentrations with more high-speed fluid per unit volume. Apparently, forcing the layer causes the entrainment ratio (as defined by Dimotakis (1986)) into the layer, which is already asymmetric in favor of the high-speed side (Koochesfahani (1984)), to be further biased towards the high-speed side. The mechanisms at work here are not clearly understood. However, some insight may be provided by the following argument suggested by Dr. M. Koochesfahani. The entrainment model proposed by Dimotakis for a *natural* shear layer gives the entrainment ratio, E, as $E = 1 + 3.9\delta_\omega/x$, where δ_ω is the vorticity thickness, a measure of the growth of the shear layer. Therefore an increase in the growth of the layer could lead to an increase in the entrainment ratio. It remains to be shown whether or not such a relationship holds for *forced* layers, however, the trend indicated by this relation is in qualitative agreement with our findings.

The second observation is a qualitative one, for which measurements will be presented later. If the pdfs are visually inspected it is fairly easy to conclude that the total amount of mixed fluid (which is proportional to the area under each $P(\xi)$ curve excluding the pure-stream delta functions) increases when the layer is forced.

The above trends are valid for each of the forced cases except in the case when the symmetry parameter is $S = 30\%$. A comparison of this case with that of the natural layer is shown in Figure 22. This figure depicts the result that the two pdfs are almost identical.

An important quantity in our study is the mixed-fluid probability, p_m. This is obtained by integrating $p(\xi, y)$ with respect to ξ, excluding the delta functions. Thus $p_m(y)$ represents the total probability of finding mixed fluid of *any* concentration, at a given y value.

Since we have concentration information at a large number of pixel locations across the width of the layer, it is relatively easy to construct the $p_m(y)$ profiles. Figure 23 displays such profiles. It is important to note that the amount of mixed fluid in the middle of the layer is actually *reduced* upon external forcing. The area below these curves is used as our measure of the total amount of mixed fluid. This quantity is denoted by δ_m, and is called the mixed-fluid thickness. The use of the word "thickness" stems from the fact that δ_m has dimension of length.

As a measure of the local shear layer width we have used δ_1, which is the 1% width of the $p_m(y)$ profile i.e. the distance over which the bell-shaped $p_m(y)$ has dropped to 1% of its maximum value. A common measure of the shear layer width is the 'visual' thickness, δ_{vis}. It has been shown (Koochesfahani (1984)) that this is essentially equivalent to δ_1.

The following table presents δ_1, δ_m, and the ratio between these two quantities, which gives a measure of the average amount of mixed fluid per unit width of the shear layer.

Table 1. Comparison of mixed fluid thicknesses.

	$\delta_1 (mm)$	$\delta_m (mm)$	δ_m / δ_1
Natural	33.3	16.1	0.48
F=4 Hz, S=30%	34.7	17.1	0.49
F=8 Hz, S=50%	37.5	19.3	0.51
F=4 Hz, S=50%	40.5	18.3	0.45
F=4 Hz, S=70%	45.7	19.7	0.43

Note the enhanced growth rates implied by the increase in δ_1.

The mixed-fluid thickness values show that forcing has increased the total amount of mixed fluid by as much as 22% compared to the natural case. However, *the amount of mixed fluid per unit width has remained essentially constant.* This suggests that the increase in the amount of mixed fluid is not so much the result of enhanced small-scale mixing (i.e. scales larger than 200 μm) but, more simply, is due to mixing taking place over a larger width of the test-section. We also note the difference in δ_m for the 4 Hz forcing cases. This confirms what we saw in the $P(\xi)$ plots - namely that the amount of mixed fluid is dependent on the *shape* of the forcing waveform.

There are several other quantities of interest which can be derived from the pdf $p(\xi,y)$ (see Appendix). The total probability of finding pure low-speed fluid, at a given y-location in the layer, is denoted by $p_0(y)$. This profile is obtained by integrating $p(\xi,y)$ over the interval $0 < \xi < \varepsilon$. If we instead integrate over the range $1-\varepsilon < \xi < 1$, we obtain $p_1(y)$, which is the total probability of finding pure high-speed fluid at a given y-location. These profiles are shown in Figures 24 and 25, respectively. These profiles illustrate the extent to which the pure fluids are transported to their 'opposite' sides of the layer and throughout the layer in general. A noteworthy point is the somewhat 'step-like' region in some of these profiles. The 'steps' on the $p_1(y)$ curves appear to have higher probabilities associated with them compared those on the $p_0(y)$ curves. As pointed out by Koochesfahani & Dimotakis (1986) for the natural layer, this may be a legacy from the initial excess of high-speed fluid in the structures at the time of roll-up. These plots also show that there is more pure fluid (from both streams) in the middle of the layer when forcing is applied. This is probably due to the larger entrainment 'tongues' between the structures seen in the flow images of the forced cases in agreement with the observation that there is less mixed fluid in the middle of the forced layers. The average high-speed fluid concentration, $\overline{\xi}(y)$, is shown in Figure 26. The profiles for the forced conditions develop a "flat" region similar to that observed by Wygnanski *et al.* (1979A), who attributed this feature to an orderly array of vortices with fairly well mixed cores.

3.3 Comparison with Roberts' Results

To the best of the author's knowledge there is only one other experimental work giving information about the extent of mixing in a forced shear layer - namely the Ph.D. thesis of Roberts (1985). The present results are now compared with those of Roberts.

Roberts conducted his experiments in a chemically reacting liquid shear layer. The amount of mixing was manifested in a quantity called the product thickness defined as,

$$\delta_{p_2} = \frac{1}{C_{2_0}} \int_{-h}^{h} \overline{c_p}(y)\,dy, \tag{3.1}$$

where h is the test-section half-width and $\overline{c_p}(y)$ is the average product concentration given by,

$$\overline{c_p}(y) = C_{2_0} \int_{\varepsilon}^{1-\varepsilon} (1-\xi)\, p(\xi, y)\, d\xi \,, \tag{3.2}$$

and C_{2_0} is the low-speed freestream reactant concentration.

Roberts plotted his results as $(\delta_{p_2})_F / (\delta_{p_2})_N$ versus X_{WO} (introduced on page 6), where the subscripts refer to the forced and natural cases, respectively. Such plots have been reproduced in Figures 27 and 28, the former being the results from a high Re, post-transitional layer and the latter from a low Re, pre-transitional layer. The unit Reynolds number, based on the velocity difference, for each case was 4340 cm $^{-1}$ and 905 cm $^{-1}$, respectively. In the present study this value is 2000 cm $^{-1}$, which is a factor of two higher than Roberts' low Re case, but a factor of two lower than his high Re case. In our study, the layer width was $\delta_1 = 33$ mm at the measurement location ($x = 20$ cm) . The Reynolds number based on this width was 6600. According to Breidenthal (1981) this corresponds to a shear layer in the latter stages of transition. This must be kept in mind when comparing the results of the two studies.

In the present case, δ_{p_2} is computed from the pdfs as shown in the Appendix. Of course, the measurements were made using the non-reacting LIF technique which, as has already been discussed, overestimates the amount of product. However, we are interested in the *relative* changes in the mixing of the forced layer compared to the natural layer. In this context, it is felt that the comparisons are valid.

The following table summarizes the results of these computations from our data.

Table 2. Comparison of product thicknesses estimated from current data.

	X_{WO}	$\delta_1 (mm)$	$\delta_{p_2} (mm)$	$(\delta_{p_2})_F / (\delta_{p_2})_N$
Natural	-	33.3	6.24	-
F=4 Hz, S=50%	0.9	40.5	7.33	1.17
F=8 Hz, S=50%	1.8	37.5	7.44	1.19

The last column shows the ratio of the amount of product in the forced case to that of the natural case.

As shown in Figure 27, Roberts found that in a high Re shear layer the effect of forcing was to increase the amount of product (δ_{p_2}) in region I, where the layer initially shows enhanced growth, and to decrease the amount of product thereafter, compared to the natural case. In the low Re case (Figure 28), it is not clear what can be concluded in region I, where there is a lot of scatter in his data. Beyond region I he found a consistent increase in the amount of product.

The present measurements indicate that the amount of product increases in all of the forcing cases, regardless of the region in which X_{WO} falls. We note that the discrepancy between the results of the two studies may be Reynolds number related, since this parameter has a strong effect on the production of three-dimensional small scales and the establishment of the mixing transition.

3.4 Effect of the Forcing Waveform Phase Difference

The case of $F = 4$ Hz and $S = 30\%$ is a curious one. For the large majority of the images within the full data sequence it was often difficult to distinguish this case from that of the natural layer. There are clearly identifiable large structures within the flow, reminiscent of a forced layer, but the 'randomness' which is characteristic of the natural layer is also certainly present. Earlier in this section it was seen that the cases of the natural layer and the $S = 30\%$ layer exhibit strikingly similar featues (flow visualization figures 10 & 13 and figures 15 & 19 and 22 - 25). Also, the actual values of the extent of mixing in these two cases is found to be very similar (Table 1). A possible explanation for the large difference in the results for the $S = 70\%$ and 30% cases is the following.

When each of these waveforms was analyzed for frequency content it was found that there were three main components in each. The approximate form of the forcing disturbance was

$$F(t) = A_1\sin(\omega t) + A_2\sin(2\omega t - \phi_2) + A_3\sin(3\omega t), \tag{3.3}$$

where $\omega = 4$, $A_2/A_1 = 0.25$ and $A_3/A_1 = 0.08$. The only difference between the waveforms for the $S = 30\%$ and 70% cases was that the phase difference, ϕ_2, was changed. For the $S = 70\%$ case the phase difference was π and for the $S = 30\%$ case it was 0. Recall that the natural frequency of the layer at this *downstream* location (about $x = 20$ cm) is close to 8 Hz, The first subharmonic frequency is then about 4 Hz, which is the same as the forcing frequency used. Hajj, Miksad & Powers (1991), working in a transitioning gaseous layer, found that the subharmonic mode generation was significantly altered when they changed their forcing phase difference from $\pi/2$ to $3\pi/2$. A numerical simulation by Riley & Metcalfe (1980)) showed pairing for a phase difference of 0 and a "shredding" action, where pairing was suppressed for a phase difference of π. What appears to be happening in the present case is that the important development of the subharmonic of the layer natural frequency is either being enhanced greatly (70% case) or very slightly (30% case), compared with the natural layer, with the only controlling parameter being the phase difference of the external waveform. Note that the results of Hajj *et al.* and Riley & Metcalfe were obtained working just downstream of the splitter plate tip. We now find that similar results may hold for the turbulent mixing layer farther downstream.

3.5 Future Work

The present work will be extended to include experiments with chemically reacting components. This will eliminate the problem of over-estimating the actual amount of mixing from which the passive scalar technique suffers. The effects of multi-frequency forcing will be investigated further. In addition, the effects of three-dimensional forcing on the mixing will be studied. A new facility is currently being designed which has a longer test-section and larger cross-section. This will enable higher Reynolds numbers to be achieved.

CONCLUSIONS

The conclusions from the present study are as follows.

- Forcing changes both the amount and composition of the mixed fluid. Upon forcing, the predominant (i.e. most probable) mixed-fluid concentration shifts to higher values. This implies that a higher entrainment asymmetry has been achieved. The total amount of mixed fluid increases in all of our forced cases compared to the natural layer.
- The details of the forcing waveform shape have a significant effect on the structure of the flow and on the mixing field. In particular, the phase difference between the fundamental and subharmonic forcing modes appears to have a strong influence on the flow even at some distance downstream of the splitter plate.
- The range of concentrations of mixed fluid with significant probabilities is essentially uniform across the entire transverse extent of the layer. This is in agreement with the findings of Koochesfahani (1984) for an unforced layer.
- Although the total amount of mixed fluid increased when forcing was applied, the amount of mixing per unit width of the layer remained nearly constant. If the mixing efficiency is defined as the fraction of the layer filled with mixed fluid, we infer that the mixing efficiency has not been improved, at scales larger than the current measurement resolution of 200μm.

APPENDIX

In Chapter 3 many statistical quantities were introduced mainly in words. This appendix serves merely to provide the mathematical description of these quantities and to show how they are related to the pdf of ξ, the high-speed fluid volume fraction.

The pdf of ξ, at a given y location, is denoted by $p(\xi,y)$. By definition of a pdf,

$$\int_0^1 p(\xi,y)\, d\xi = 1.$$

The average high-speed fluid concentration is then given by

$$\bar{\xi}(y) = \int_0^1 \xi p(\xi,y)\, d\xi.$$

A characteristic of these pdfs is that, in the ideal case, they possess two 'delta' functions - one at $\xi = 0$ representing pure (unmixed) low-speed fluid, and one at $\xi = 1$, indicating pure high-speed fluid. Of course, in practice, a finite width, ε, is associated with these delta functions. The value of ε is dictated by the overall signal-to-noise ratio in the measurement and, in the present case, was about 0.047. Thus, concentrations in the range $0 \leq \xi < \varepsilon$ are treated as pure low-speed fluid, whereas the range $1-\varepsilon < \xi \leq 1$ corresponds to pure high-speed fluid. Mixed fluid is then indicated by the range $\varepsilon \leq \xi \leq 1-\varepsilon$.

We can then define the probabilities p_0 and p_1 of finding pure low- and high-speed fluid, respectively, as

$$p_0(y) = \int_0^{\varepsilon} p(\xi,y)\, d\xi \quad , \qquad p_1(y) = \int_{1-\varepsilon}^{1} p(\xi,y)\, d\xi.$$

One of the most important quantities in the present work is the probability of finding mixed fluid (at *any* concentration). This quantity is found by integrating

$p(\xi,y)$ over the range of mixed fluid concentrations, i.e.

$$p_m(y) = \int_{\varepsilon}^{1-\varepsilon} p(\xi,y)\, d\xi .$$

We constructed each p_m curve in the following way. Pdfs $p(\xi,y)$ were obtained at 11 y-locations across the layer. These were integrated over the range $\varepsilon \le \xi \le 1-\varepsilon$ yielding 11 values of the $p_m(y)$ curve. These data points were then fitted with an exponential curve. [Note that a value of p_m which is less than unity indicates the presence of unmixed fluid.]

The reference location y = 0 in this study in this study was arbitrarily chosen to coincide with the point at which p_m became a maximum. The curve p_m also served to define our reference thickness δ_1, which is known to be within 5% of the layer visual thickness (Koochesfahani & Dimotakis (1986)). The thickness, δ_1 was defined to be the 1% width of the p_m profile i.e. the width over which p_m had dropped to 1% of its maximum value.

One of the most important properties of $p(\xi,y)$ is that the distribution of its mixed-fluid part (i.e. excluding the delta functions) has a similar shape for all the y locations across the width of the layer. This allows the layer to be characterized by a single pdf, namely the averaged pdf :

$$P(\xi) = \frac{1}{2h} \int_{-h}^{h} p(\xi,y)dy ,$$

where h is the half-width of the test-section. The total amount of mixed fluid across the layer is given by the mixed fluid thickness, δ_m, defined by

$$\delta_m = \int_{-h}^{h} p_m(y)dy = \int_{-h}^{h} \int_{\varepsilon}^{1-\varepsilon} p(\xi,y)\, d\xi\, dy ,$$

which is the area under the mixed fluid probability curve.

In chemically reacting shear layers, the product thickness is often used as a measure of the extent of mixing. For fast chemical reactions, in the limit of large and small stoichiometric mixture fractions (Koochesfahani & Dimotakis (1986)), two product thicknesses are defined as

$$\delta_{p_1} = \int_{-h}^{h} \int_{\varepsilon}^{1-\varepsilon} \xi p(\xi, y)\, d\xi\, dy \quad , \qquad \delta_{p_2} = \int_{-h}^{h} \int_{\varepsilon}^{1-\varepsilon} (1-\xi) p(\xi, y)\, d\xi\, dy.$$

By simply adding these the two quantities we get back the mixed fluid thickness,

$$\delta_m = \delta_{p_1} + \delta_{p_2}.$$

We note that Roberts (1985) used the product thickness δ_{p_2} for his results.

REFERENCES

BALLINT, J.L., WALLACE, J.M. & VUKOSLAVCEVIC, P. 1988 The statistical properties of the vorticity field of a two-stream turbulent mixing layer. *Proc. 2nd European Turbulence Conference, Berlin, Germany.*

BERNAL, L.P. 1981 The coherent structure of turbulent mixing layers. PhD thesis, California Institute of Technology, Pasadena, CA.

BREIDENTHAL, R.E. 1978 A chemically reacting turbulent shear layer. PhD thesis, California Institute of Technology, Pasadena, CA.

BREIDENTHAL, R.E. 1980 Response of plane shear layers and wakes to strong three-dimensional disturbances. *Phys. Fluids* **23**(10), 1929-1934.

BREIDENTHAL, R.E. 1981 Structure in turbulent mixing layers and wakes using a chemical rection. *J. Fluid Mech.* **109**, 1-24.

BROWN, G.L. & ROSHKO, A. 1971 The effect of density difference on the turbulent mixing layer. *Turbulent Shear Flows*, AGARD-CP-93, 23.1-23.12.

BROWN, G.L. & ROSHKO, A. 1974 On density effects and large structure in turbulent mixing layers. *J. Fluid Mech.* **64**, 775-816.

BROWAND, F.K. 1966 An experimental investigation of the instability of an incompressible, separated shear layer. *J. Fluid Mech.* **26**, 281-307.

BROWAND, F.K. & HO, C.M. 1983 The mixing layer : an example of quasi two-dimensional turbulence. *J. de Mécanique Théorique et Appliquée Numéro Spécial*, 99-120.

BROWAND, F.K. & WEIDMAN, P.D. 1976 Large scales in the developing mixing layer. *J. Fluid Mech.* **76**, 127-144.

DIMOTAKIS, P.E. 1986 Two dimensional shear layer entrainment. *AIAA J.* **24(11)**, 1791-1796.

DIMOTAKIS, P.E., & BROWN, G.L. 1976 The mixing layer at high Reynolds number : large-structure dynamics and entrainment. *J. Fluid Mech.* **78**, 535-560.

FOSS, J.F. & HAW, R.C. 1990 Vorticity and velocity measurements in a 2:1 mixing layer. *Forum on Turbulent Flows*, **94**, 115-120.

FOSS, J.F. & WALLACE, J.M. 1989 The measurement of vorticity in transitional and fully developed turbulent flows. *Advances in Fluid Mechanics Measurements* (ed. M. Gad-el-Hak). Lecture Notes in Engineering, **45**. Springer-Verlag.

FREYMUTH, P. 1966 On transition in a separated laminar boundary layer. *J. Fluid Mech.* **25**, 683-704.

HAJJ, M.R., MIKSAD, R.W. & POWERS, E.J. 1991 Experimental investigation of the fundamental-subharmonic coupling : effect of the initial phase difference. *AIAA Paper* no. 91-0624, *29th Aerospace Sciences Meeting, Reno, Nevada, January 7-10.*

HO, C.M. & HUANG, L.S. 1982 Subharmonics and vortex merging in mixing layers. *J. Fluid Mech.* **119**, 443-473.

HO, C.M. & HUERRE, P. 1984 Perturbed free shear layers. *Ann. Rev. Fluid Mech.* **16**, 365-424.

HUANG, L.S. & HO, C.M. 1990 Small-scale transition in a plane mixing layer. *J. Fluid Mech.* **210**, 475-500.

JIMENEZ, J., MARTINEZ-VAL, R. & REBOLLO, M. 1979 On the origin and evolution of three-dimensional effects in the mixing layer. *Final Report* DA-ERO 79-G-079, Universidad Politecnica de Madrid, Spain.

KONRAD, J.H. 1976 An experimental investigation of mixing in two-dimensional turbulent shear flows with applications to diffusion-limited chemical reactions. PhD thesis, California Institute of Technology, Pasadena, CA; and *Project SQUID Technical Report* CIT-8-PU.

KOOCHESFAHANI, M.M 1984 Experiments on turbulent mixing and chemical reactions in a liquid mixing layer. PhD thesis, California Institute of Technology, Pasadena, CA.

KOOCHESFAHANI, M.M. & DIMOTAKIS, P.E. 1985 Laser induced fluorescence measurements of mixed fluid concentration in a liquid plane shear layer. *AIAA J.* **23**, 1700-1707.

KOOCHESFAHANI, M.M. & DIMOTAKIS, P.E. 1986 Mixing and chemical reactions in a turbulent liquid mixing layer. *J. Fluid Mech.* **170**, 83-112.

LANG, D.B. 1985 Laser doppler velocity and vorticity measurements in turbulent shear layers. PhD thesis, California Institute of Technology, Pasadena, CA.

LASHERAS, J.C., CHO, J.S. & MAXWORTHY, T. 1986 On the origin and evolution of streamwise vortical structures in a plane, free shear layer. *J. Fluid Mech.* **172**, 231-258.

LASHERAS, J.C., CHOI, H. 1988 Three-dimensional instability of a plane, free shear layer : an experimental study of the formation and evolution of streamwise vortices. *J. Fluid Mech.* **189**, 53-86.

MICHALKE, A. 1965 On spatially growing disturbances in an inviscid shear layer. *J. Fluid Mech.* **23**, 521-544.

MIKSAD, R.W. 1972 Experiments on the nonlinear stages of free shear layer transition. *J. Fluid Mech.* **56**, 695-719.

MILLER, P.L. & DIMOTAKIS, P.E. 1991 Stochastic geometric properties of scalar interfaces in turbulent jets. *Phys. Fluids* **3(1)**, 168-177.

MOSER, R.D. & ROGERS, M.M 1990 Mixing transition and the cascade to small scales in a plane mixing layer. *Proc. of IUTAM Symposium Stirring and Mixing, La Jolla, California, August 20-24*.

NYGAARD, K.J. & GLEZER, A. 1991 Evolution of streamwise vortices and generation of small-scale motion in a plane mixing layer. Submitted to *J. Fluid Mech.*

OSTER, D. & WYGNANSKI, I. 1982 The forced mixing layer between parallel streams. *J. Fluid Mech.* **123**, 91-130.

REBOLLO, M. 1973 Analytical and experimental investigation of a turbulent mixing layer of different gases in a pressure gradient. PhD thesis, California Institute of Technology, Pasadena, CA.

RILEY, J.J. & METCALFE, R.W. 1980 Direct numerical simulation of a perturbed, turbulent mixing layer. *AIAA paper*, no. 80-0274.

ROBERTS, F.A. 1985 Effects of a periodic disturbance on structure and mixing in turbulent shear layers and wakes. PhD thesis, California Institute of Technology, Pasadena, CA.

ROSHKO, A. 1976 Structure of turbulent shear flows : a new look. *AIAA J.* **14**, 1349-1357.

ROSHKO, A. 1990 The mixing transition in free shear flows. *Proc. NATO Advance Research Workshop on THE GLOBAL GEOMETRY OF TURBULENCE (Impact of nonlinear dynamics), Rota (Cádiz), Spain, July 8-14.*

WINANT, C.D. & BROWAND, F.K. 1974 Vortex pairing : the mechanism of turbulent mixing layer growth at moderate Reynolds number. *J. Fluid Mech.* **63**, 237-255.

WYGNANSKI, I., OSTER, D. & FIEDLER, H. 1979A A forced, turbulent mixing layer : A challenge for the predictor. *Turbulent Shear Flows 2 : 2nd Intl. Symp. Turbulent Shear Flows, London, July 2-4*, pp. 314-326.

WYGNANSKI, I., OSTER, D., FIEDLER, H. & DZIOMBA, B. 1979B On the perseverence of a quasi-two-dimensional eddy-structure in a turbulent mixing layer. *J. Fluid Mech.* **92**, 1-16.

ZAMAN, K.B.M.Q. & HUSSAIN, A.K.M.F. 1981 Turbulence suppression in free shear flows by controlled excitation. *J. Fluid Mech.* **103**, 133-159.

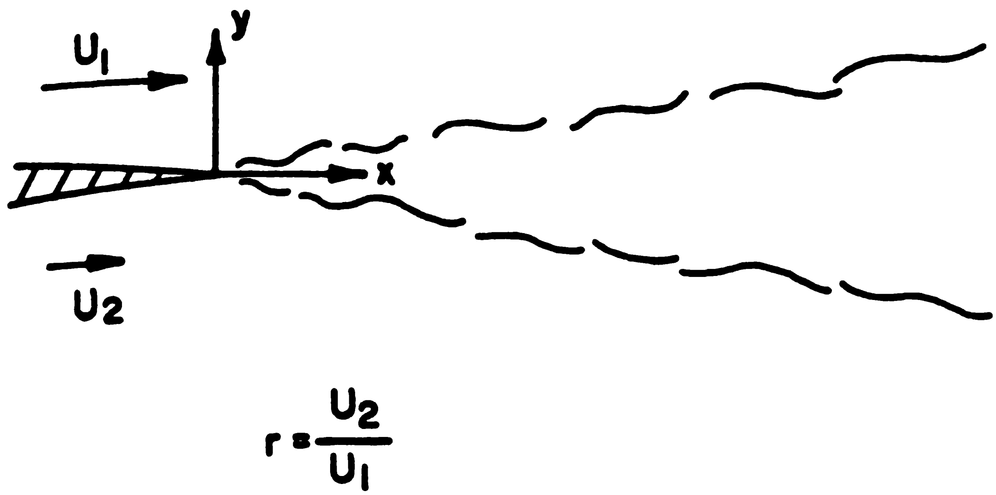

Figure 1. Shear layer configuration.

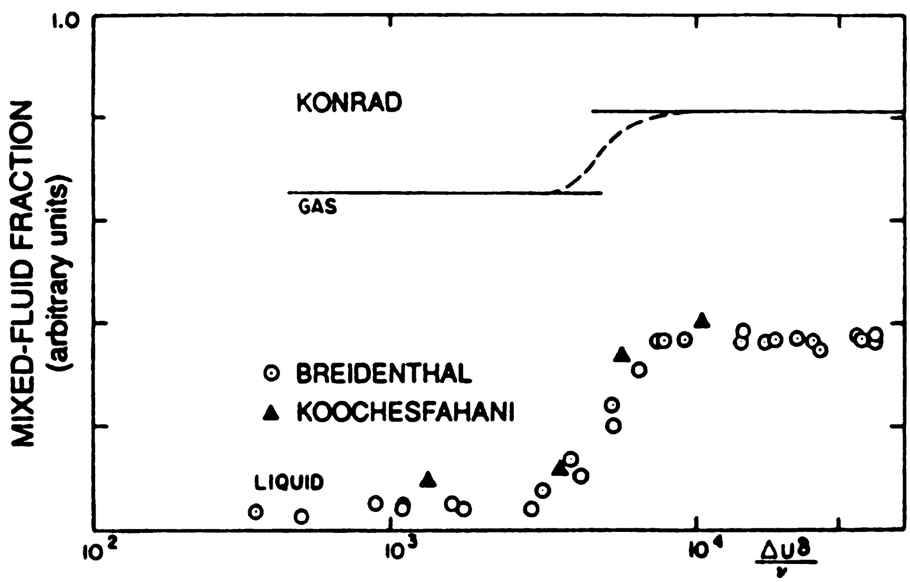

Figure 2. The mixing transition.

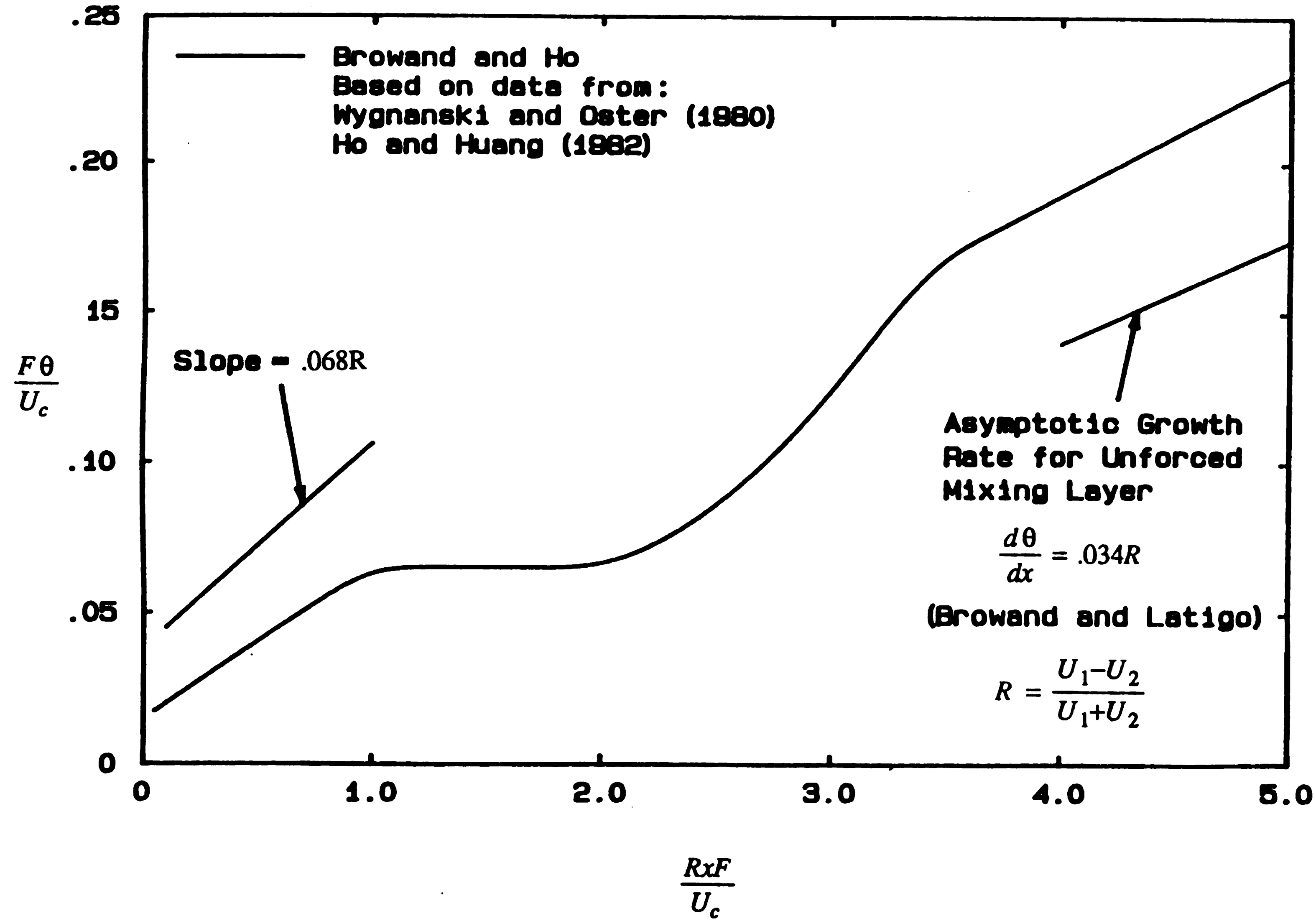

Figure 3. Effect of forcing on shear layer growth (from Roberts (1985)).

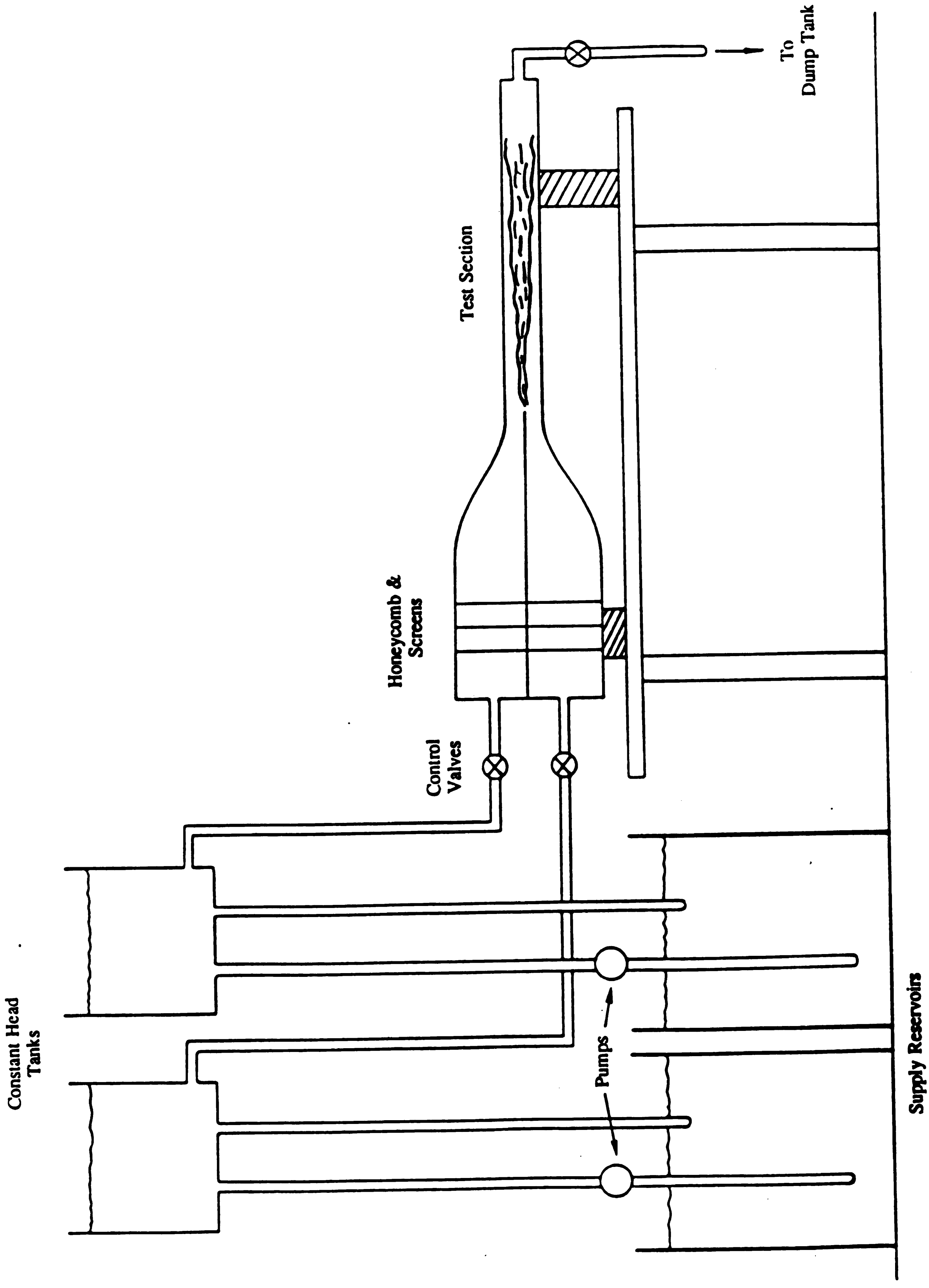

Figure 4. Shear layer facility.

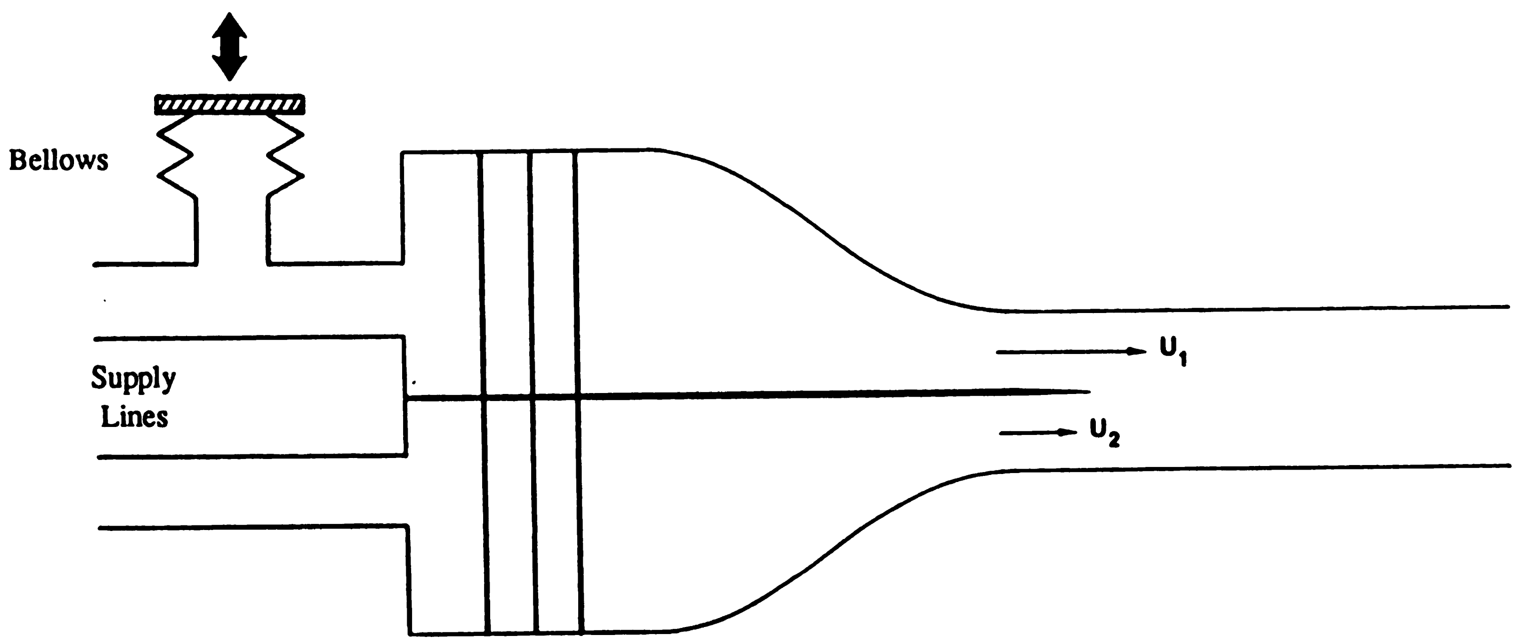

Figure 5. **Shear layer forcing mechanism.**

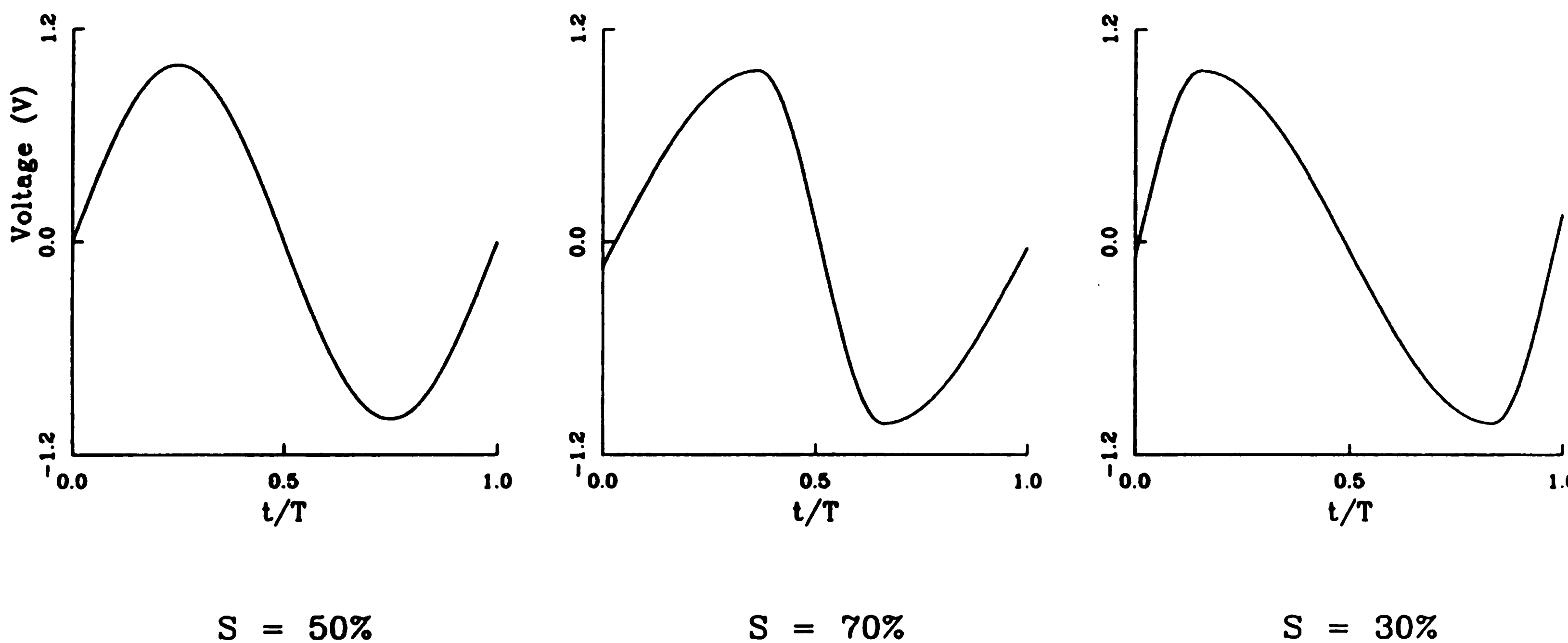

Figure 6. Forcing waveform profiles.

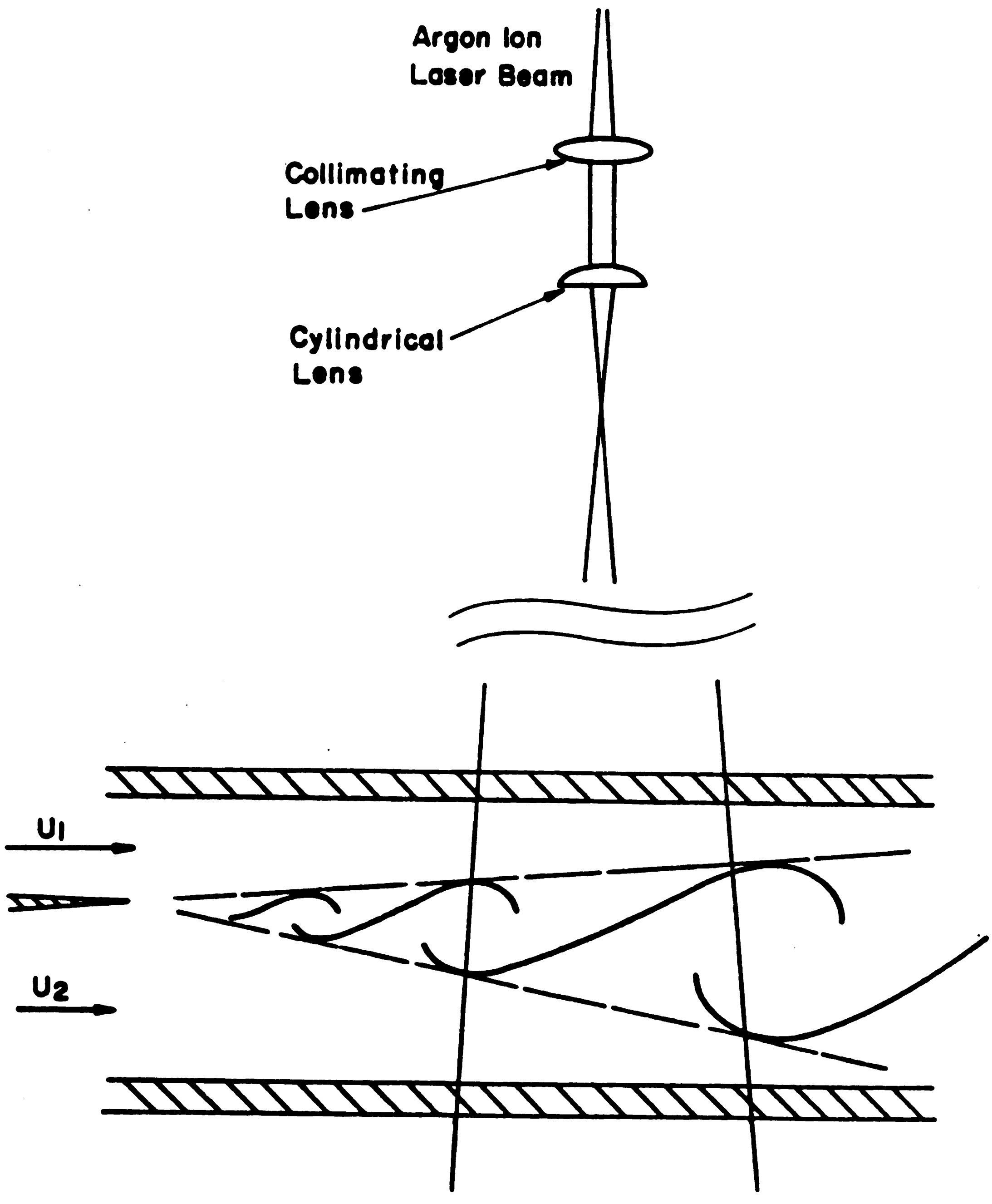

Figure 7. Laser sheet illumination setup.

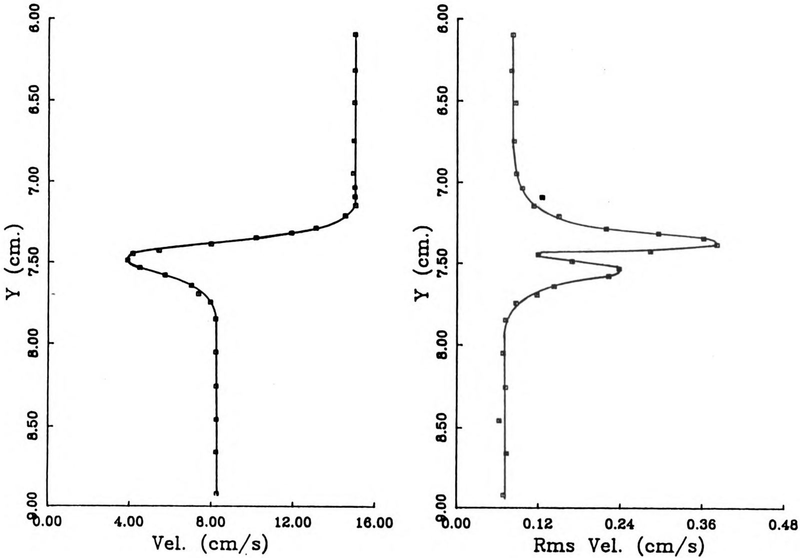

Figure 8. Mean and rms velocity profiles of the natural shear layer at $x \approx 1$ cm.

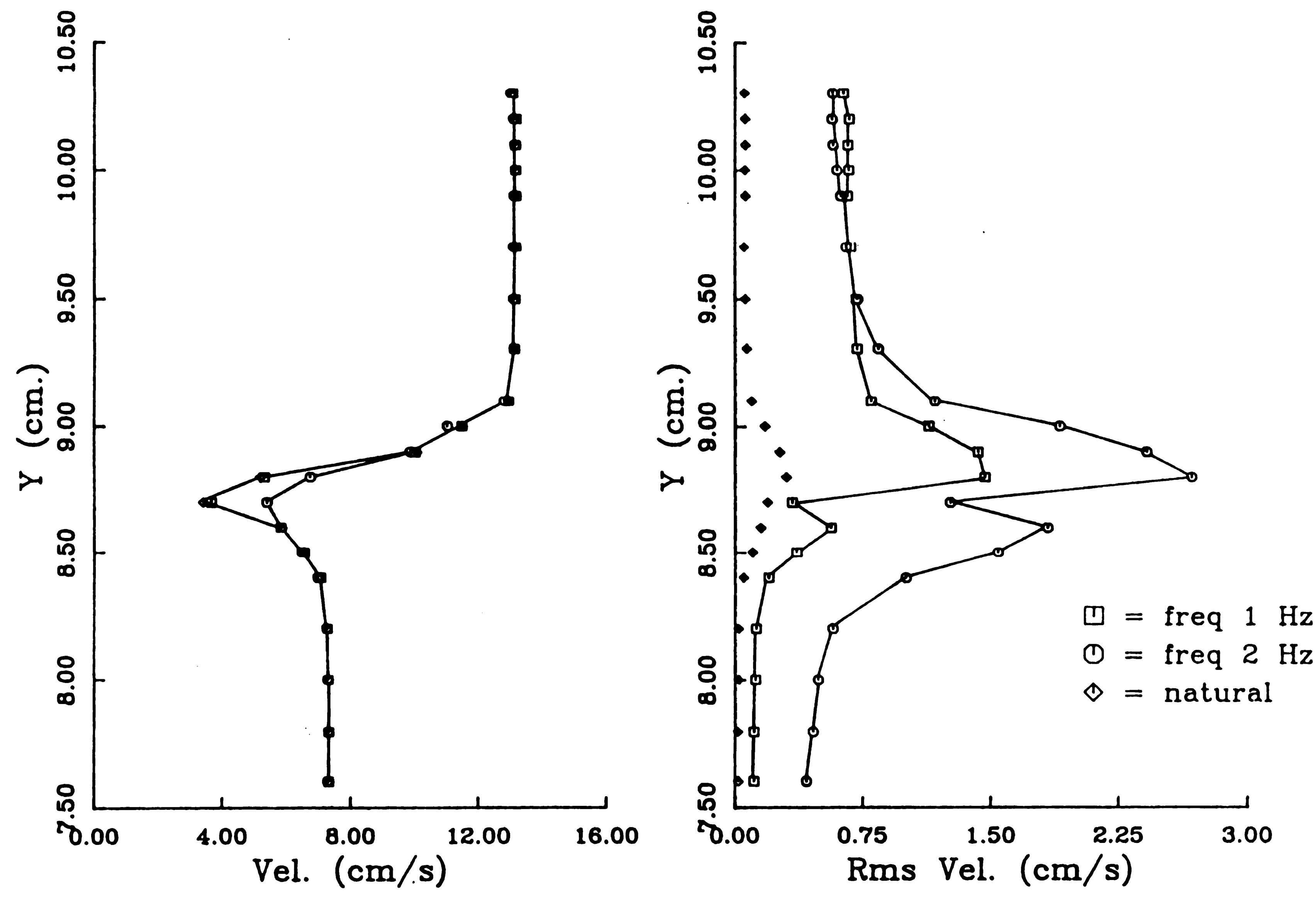

Figure 9. Effect of large perturbation amplitude (≈ 14%) on the mean and rms velocity profiles at $x \approx 1$ cm.

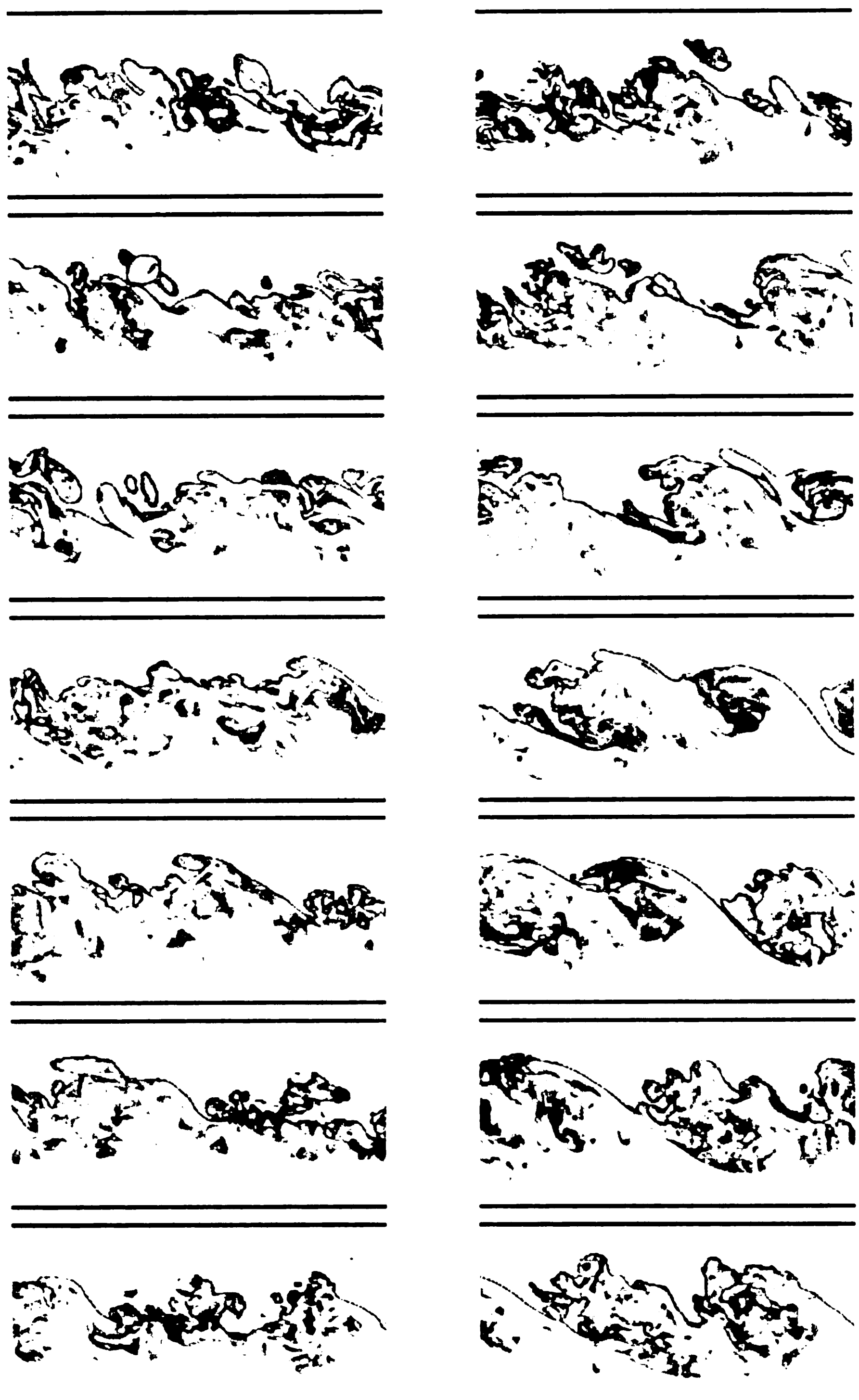

Figure 10. Digital LIF image time sequence of the mixing field for the natural layer. Flow is from right to left and top to bottom (Δt = 1/15 sec).

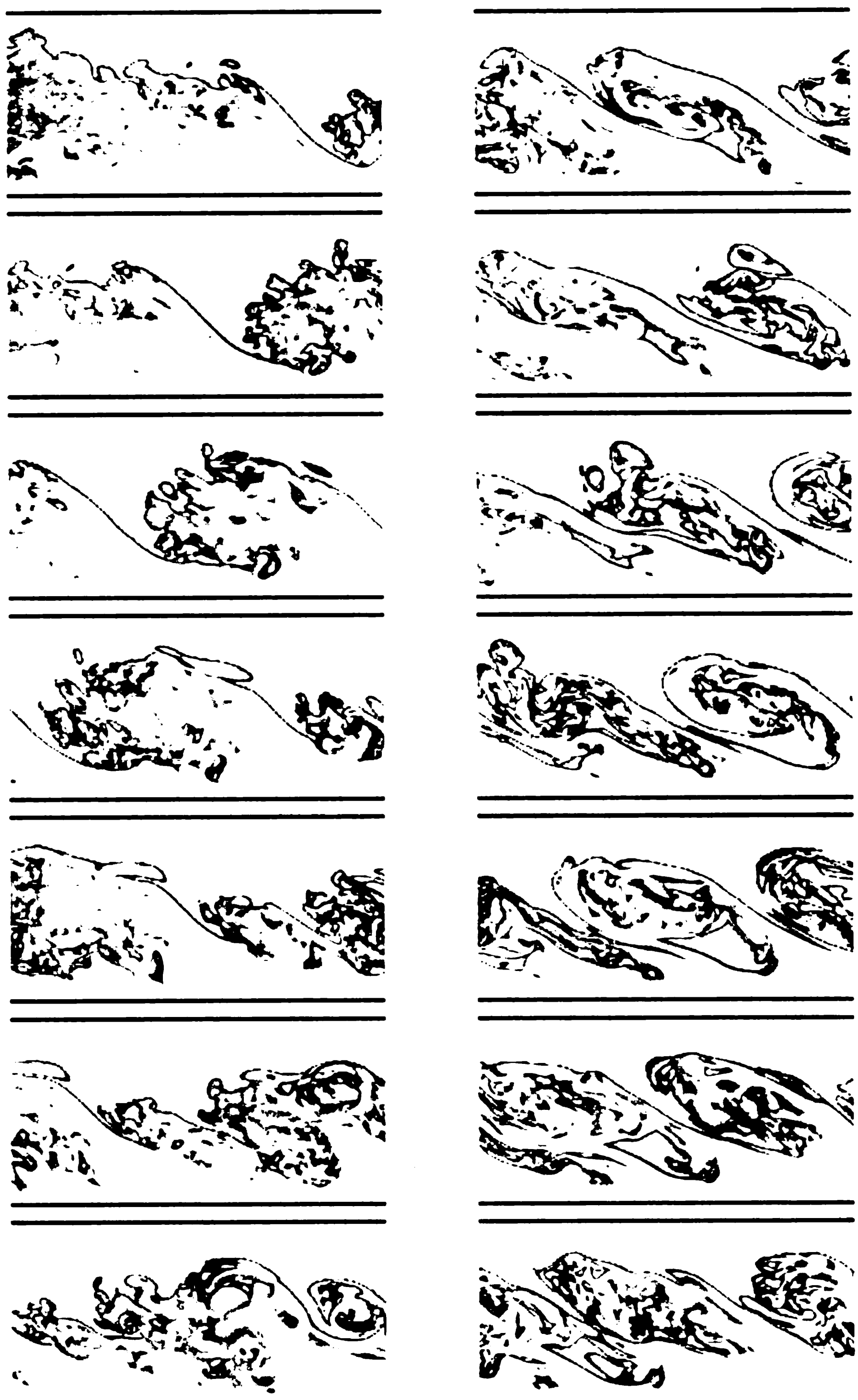

Figure 11. Mixing field for sinusoidal forcing F = 4 Hz (left) and F = 8 Hz cases.

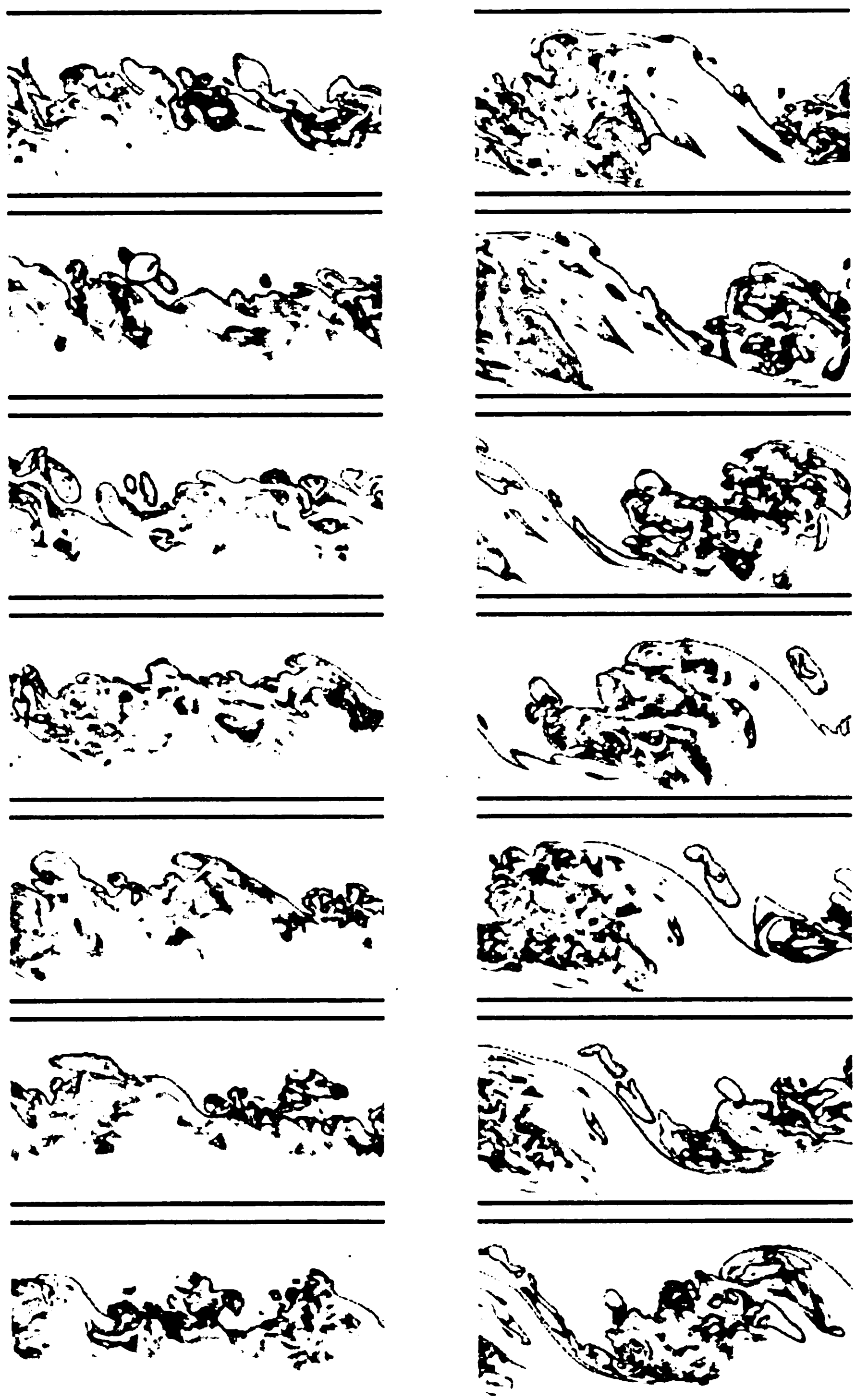

Figure 12. Mixing field for non-sinusoidal forcing at F = 4 Hz, S = 70% (right) compared with the natural case.

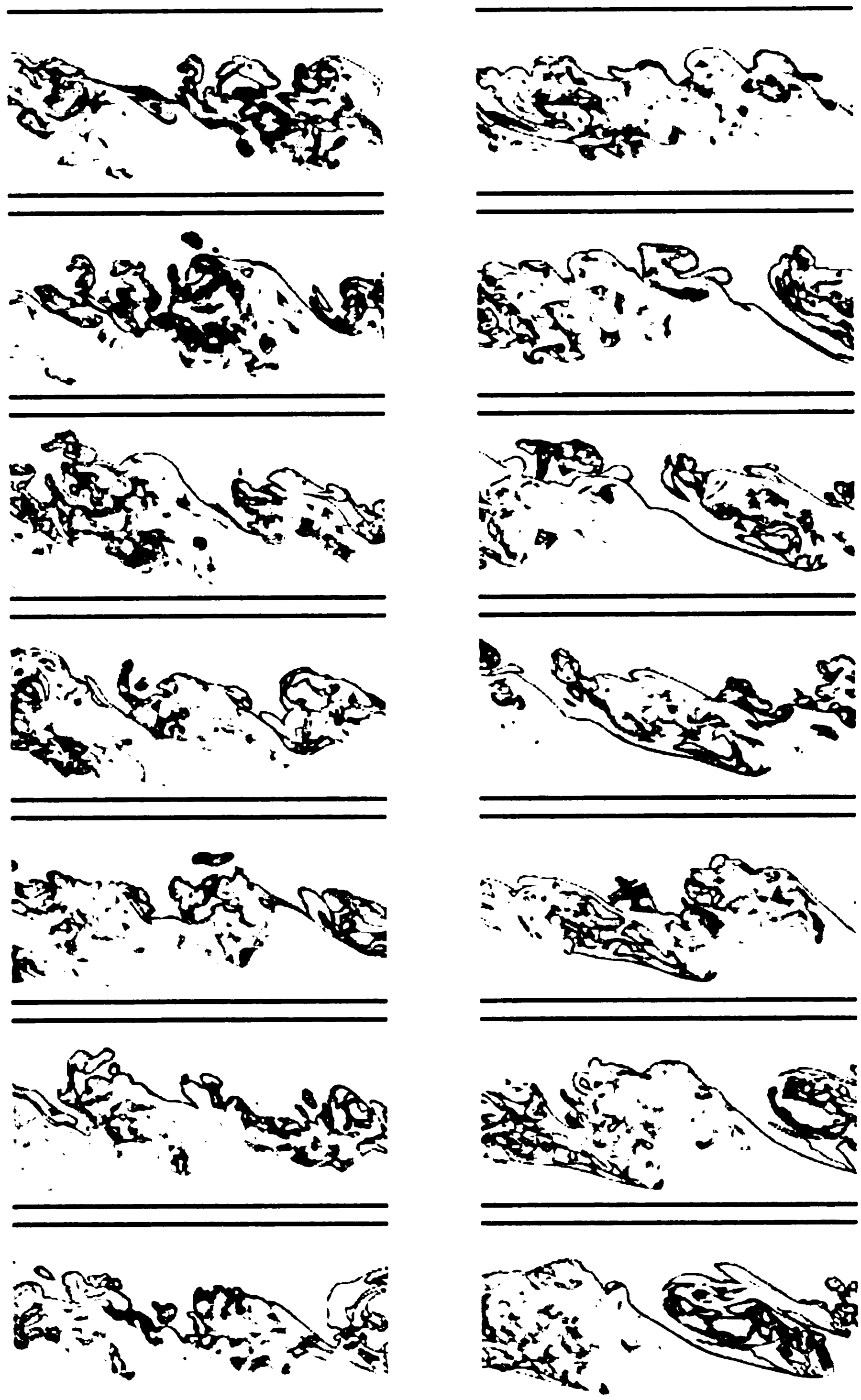

Figure 13. Mixing field for non-sinusoidal forcing at $F = 4$ Hz, $S = 30\%$ (not continuous sequences).

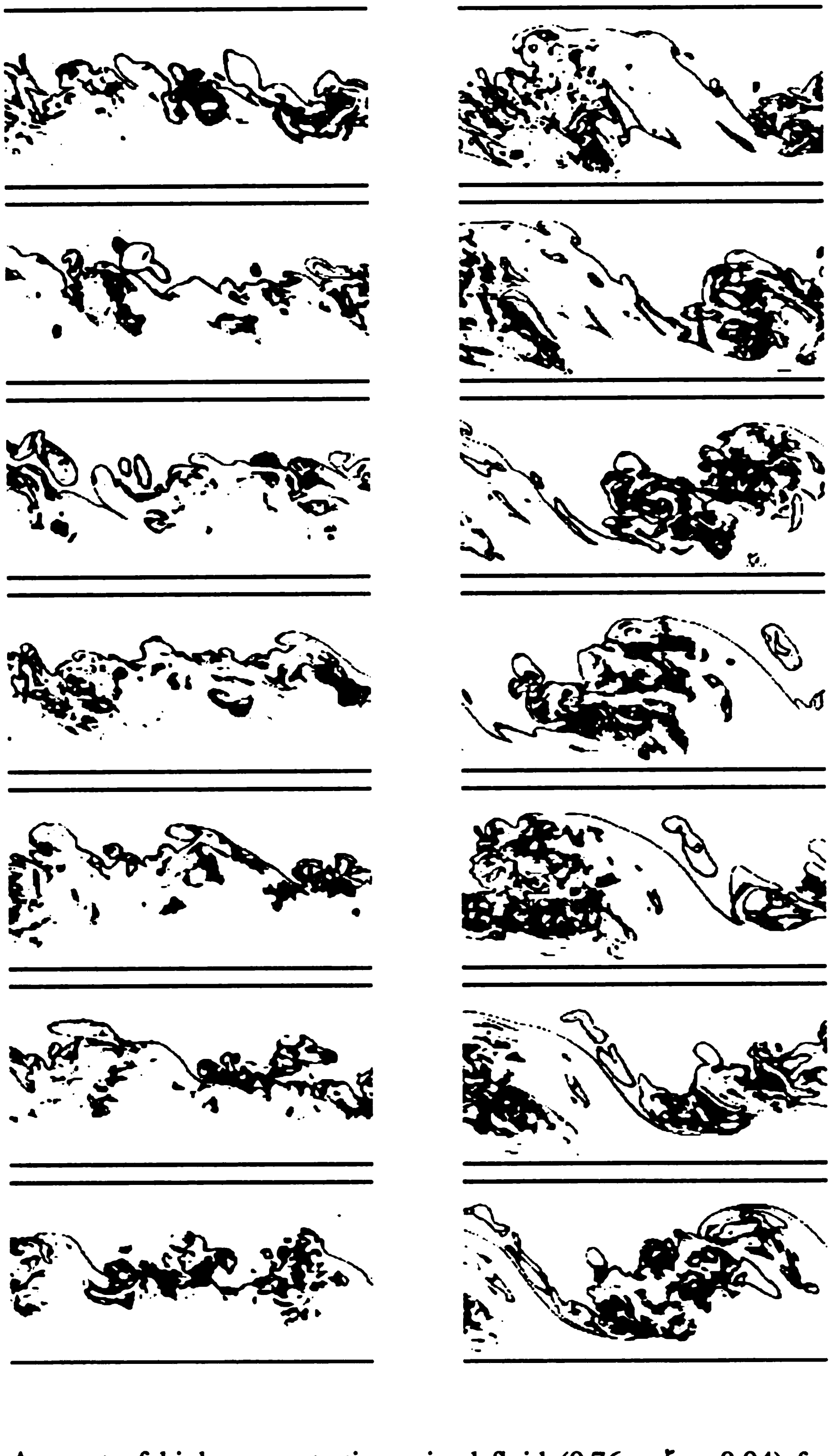

Figure 14. Amount of high concentration mixed fluid ($0.76 < \xi < 0.94$) for the non-sinusoidal $F = 4$ Hz, $S = 70\%$ case (right) compared with the natural case.

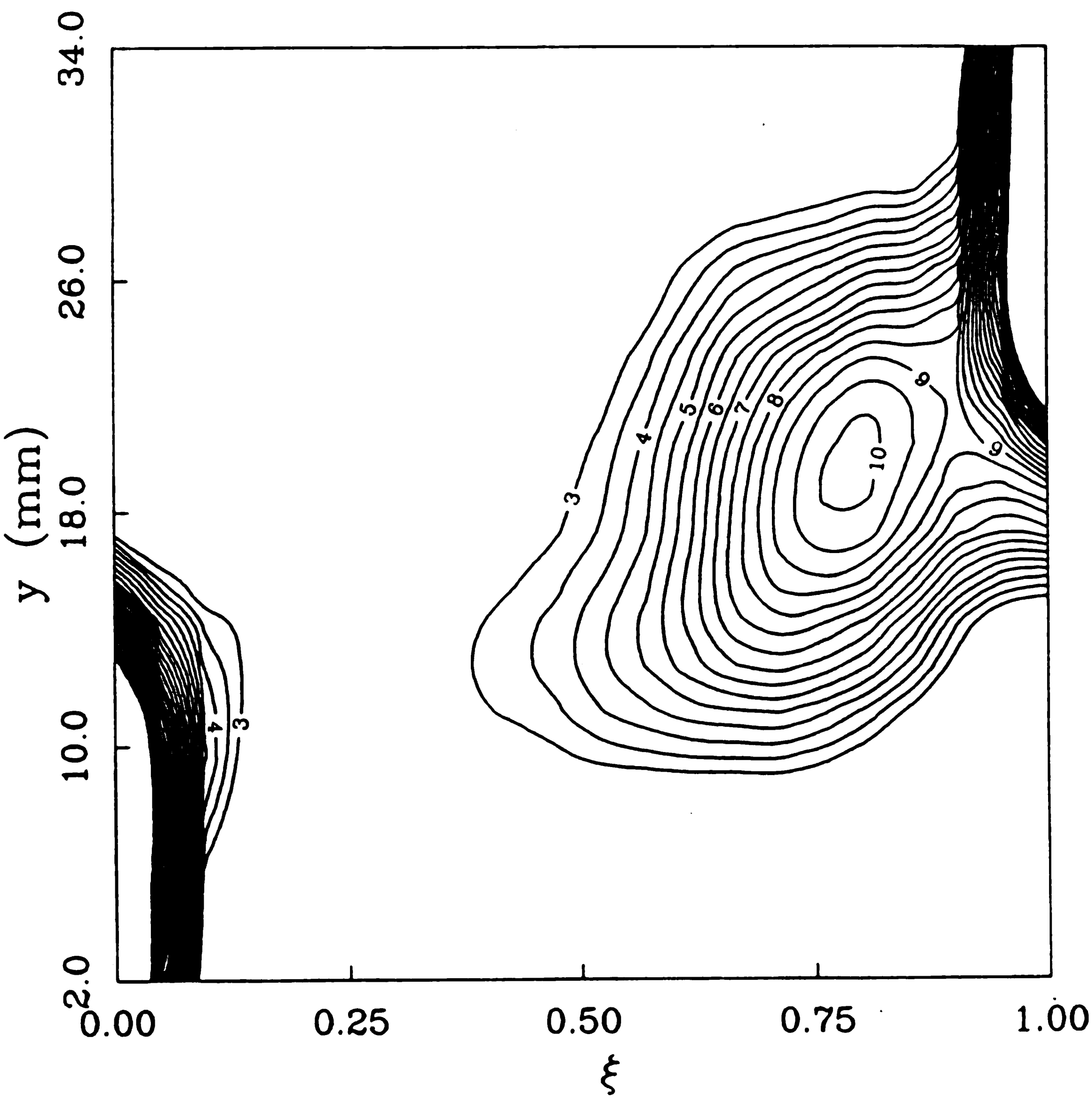

Figure 15. Contour plot of the composition distribution $p(\xi, y)$ at $x \approx 20$ cm for the natural case.

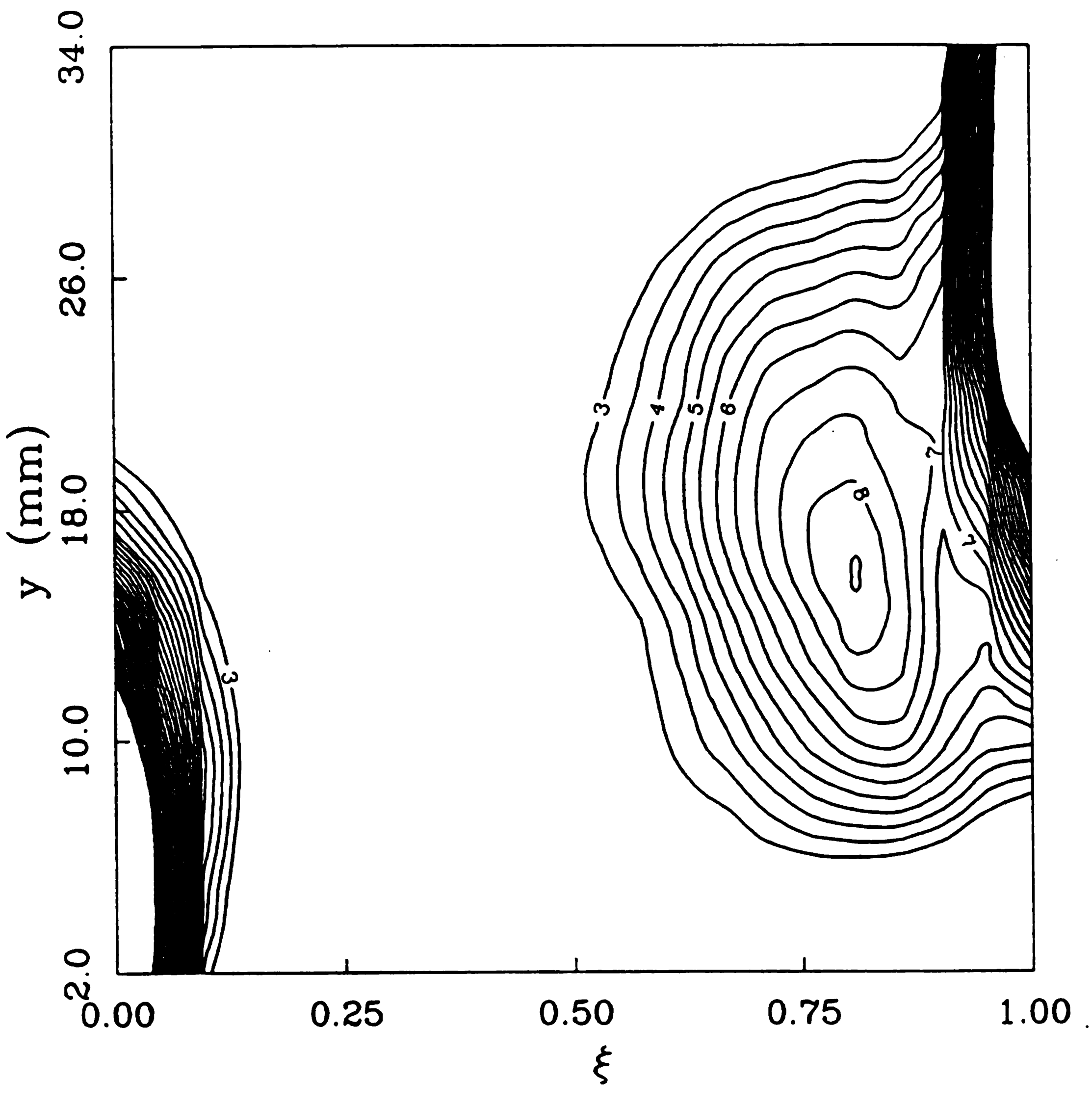

Figure 16. Composition distribution for sinusoidal forcing at $F = 4$ Hz.

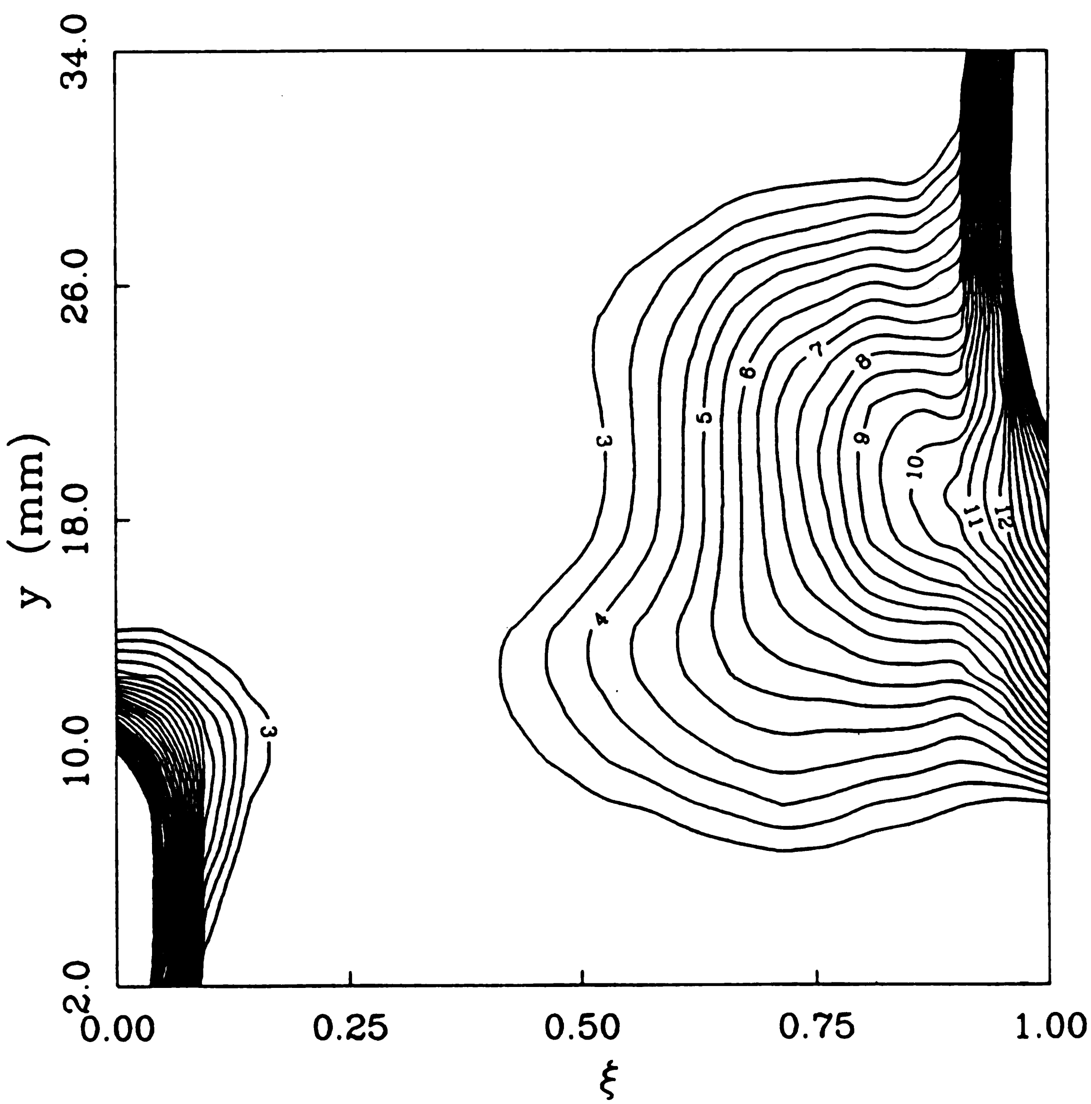

Figure 17. Composition distribution for sinusoidal forcing at F = 8 Hz.

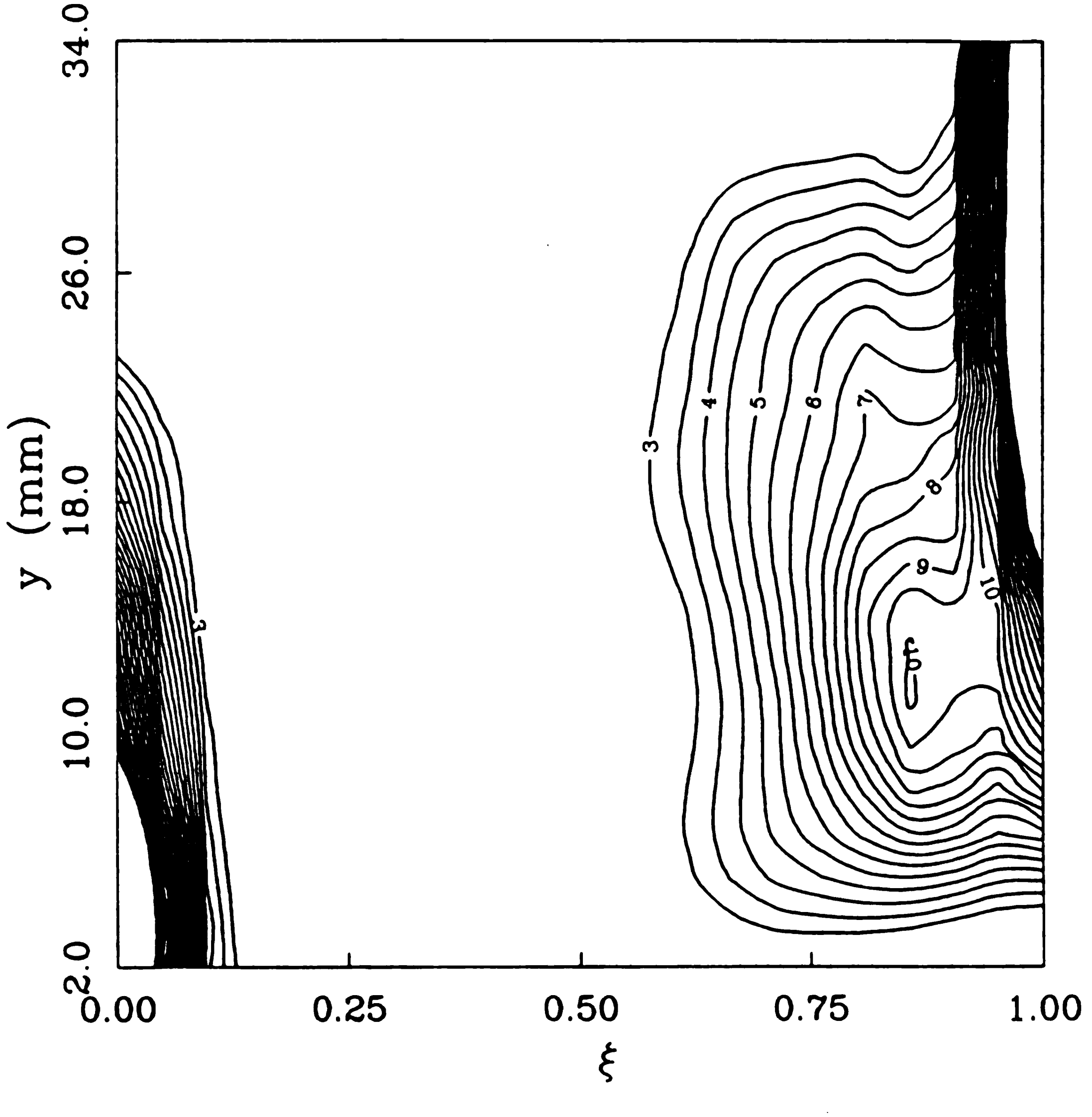

Figure 18. Composition distribution for non-sinusoidal forcing at F = 4 Hz, S = 70%.

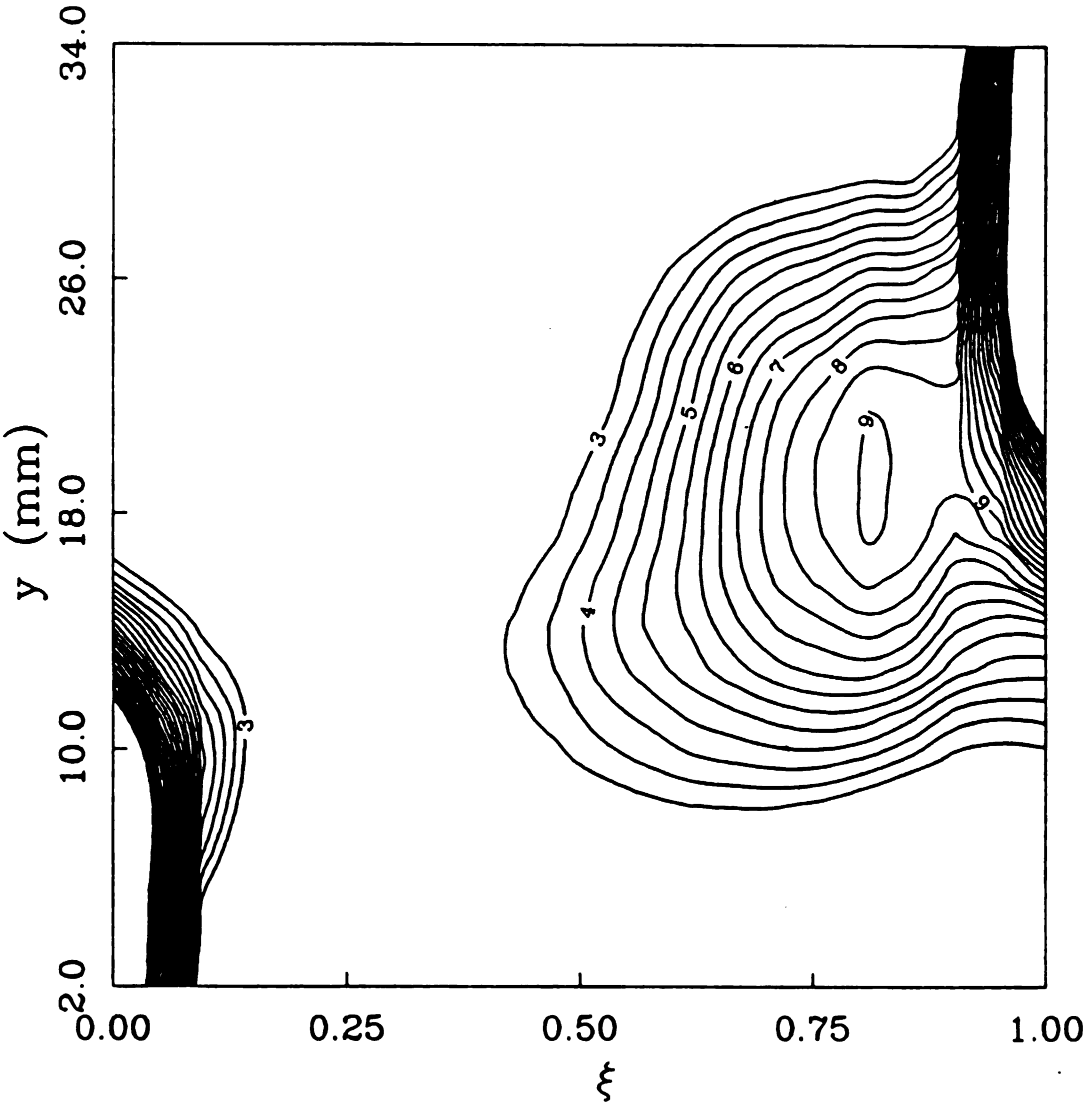

Figure 19. Composition distribution for non-sinusoidal forcing at F = 4 Hz, S = 30%.

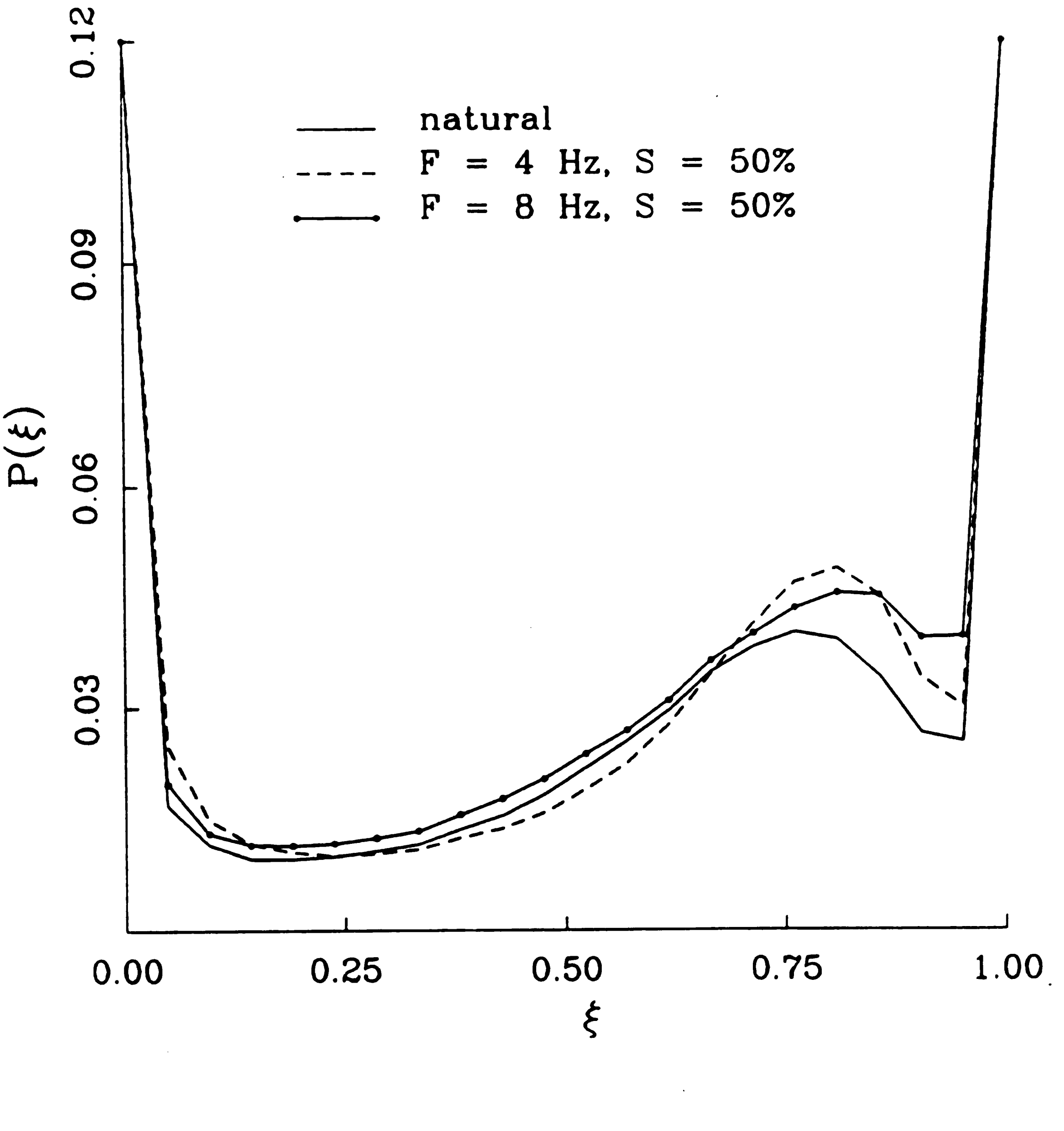

Figure 20. Effect of sinusoidal forcing on the averaged pdf concentration field, $P(\xi)$.

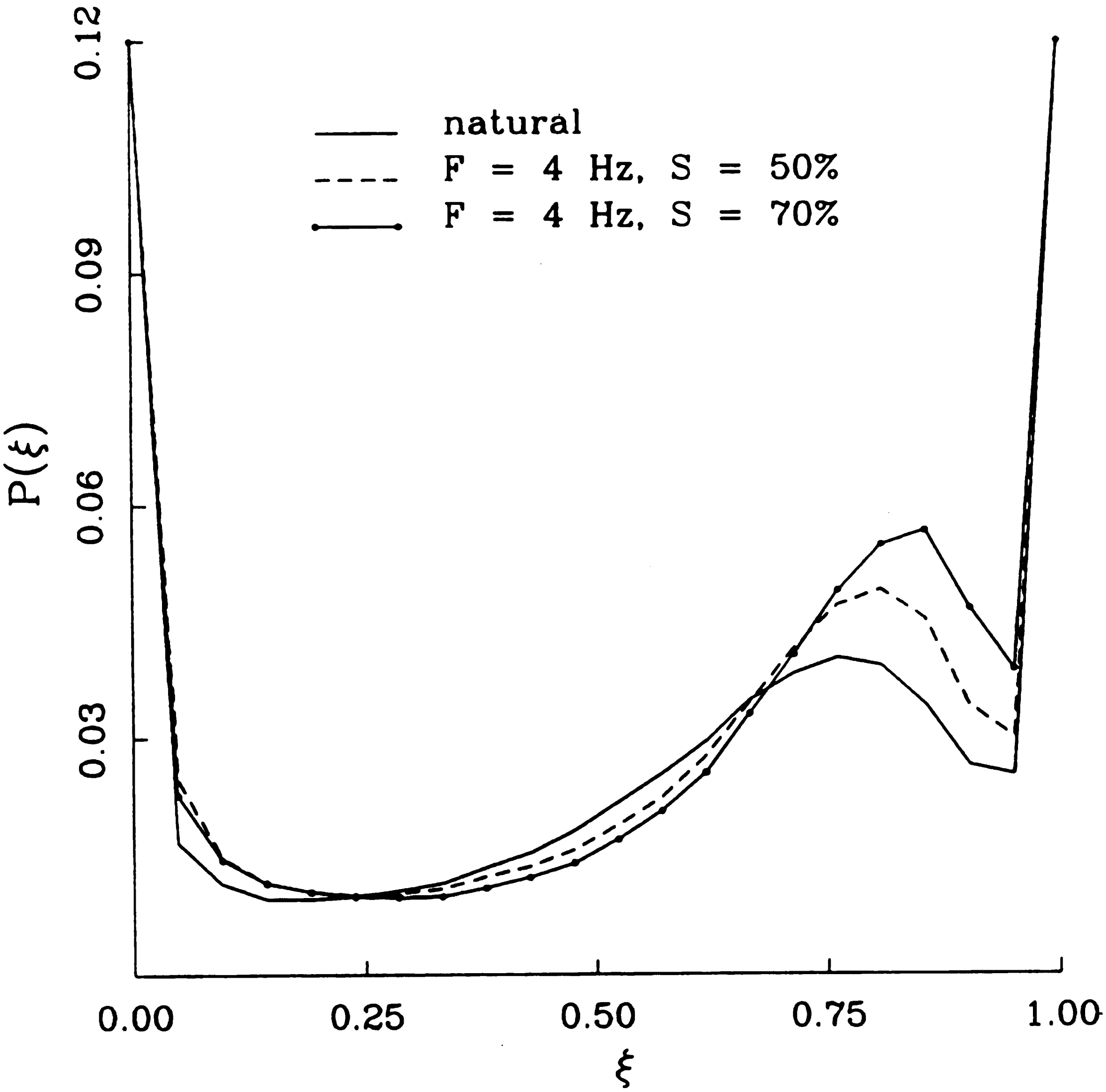

Figure 21. Effect of non-sinusoidal forcing at $F = 4$ Hz, $S = 70\%$ on $P(\xi)$.

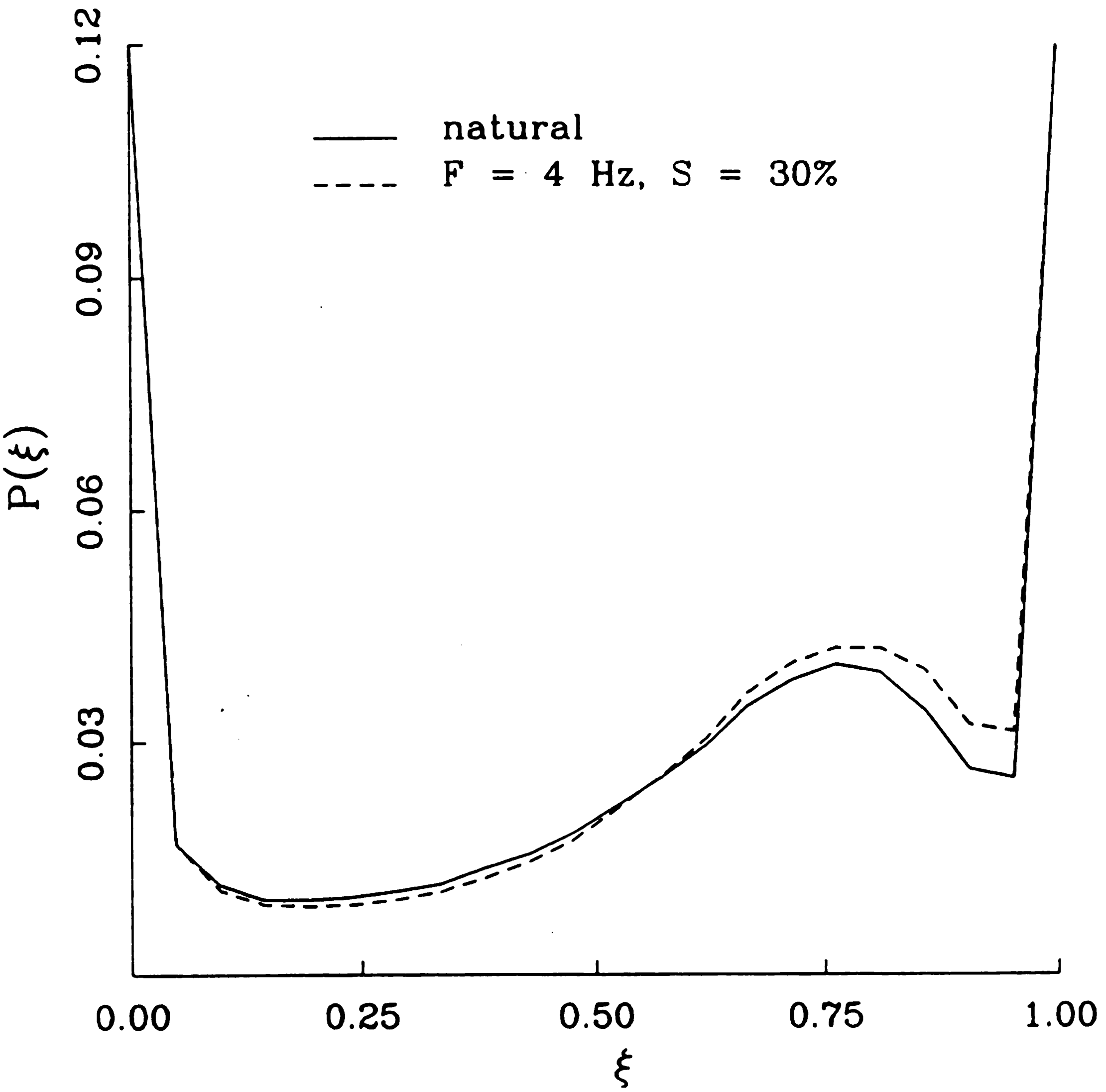

Figure 22. Effect of non-sinusoidal forcing at $F = 4$ Hz, $S = 30\%$ on $P(\xi)$.

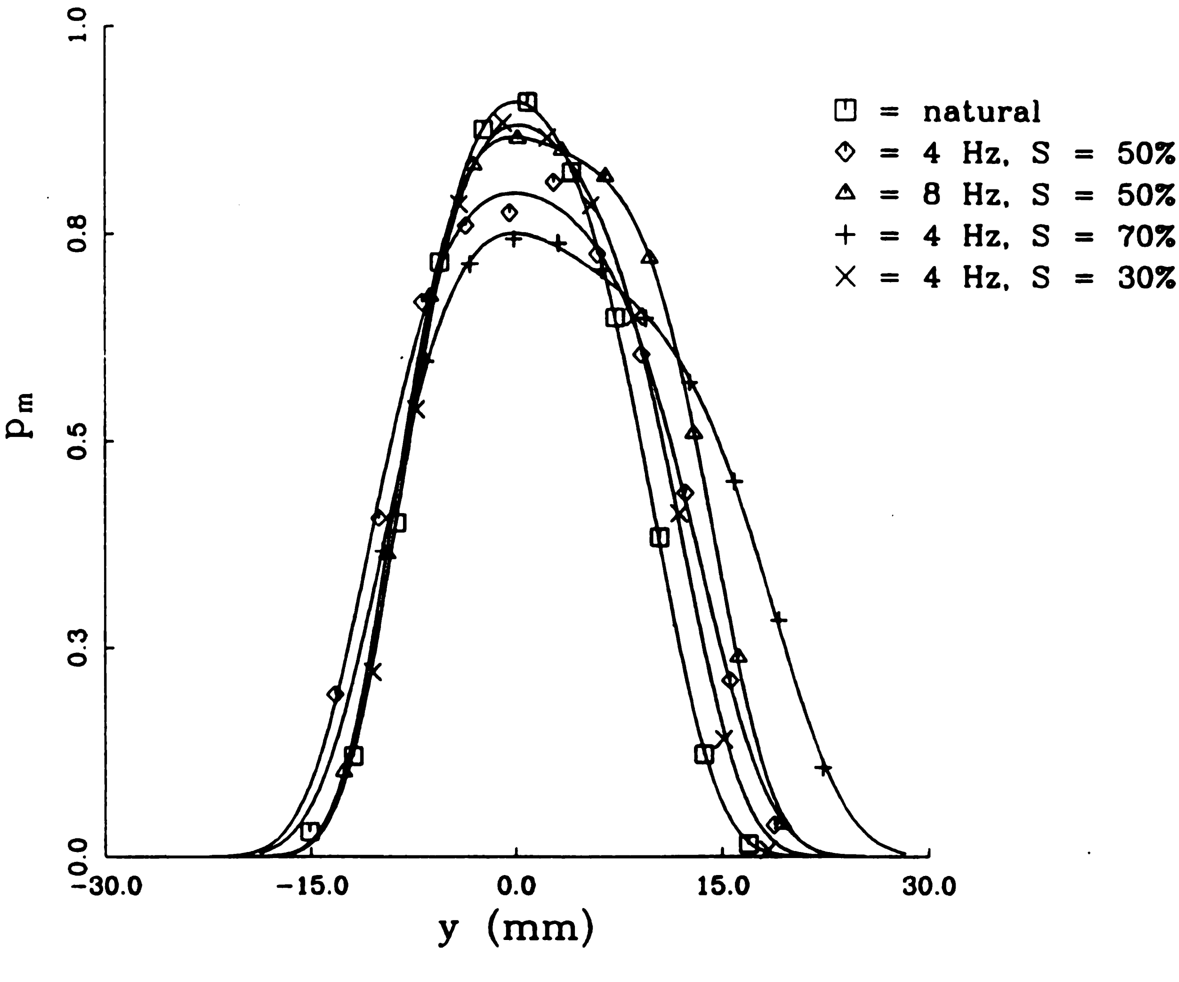

Figure 23. Transverse profiles of total mixed-fluid probability.

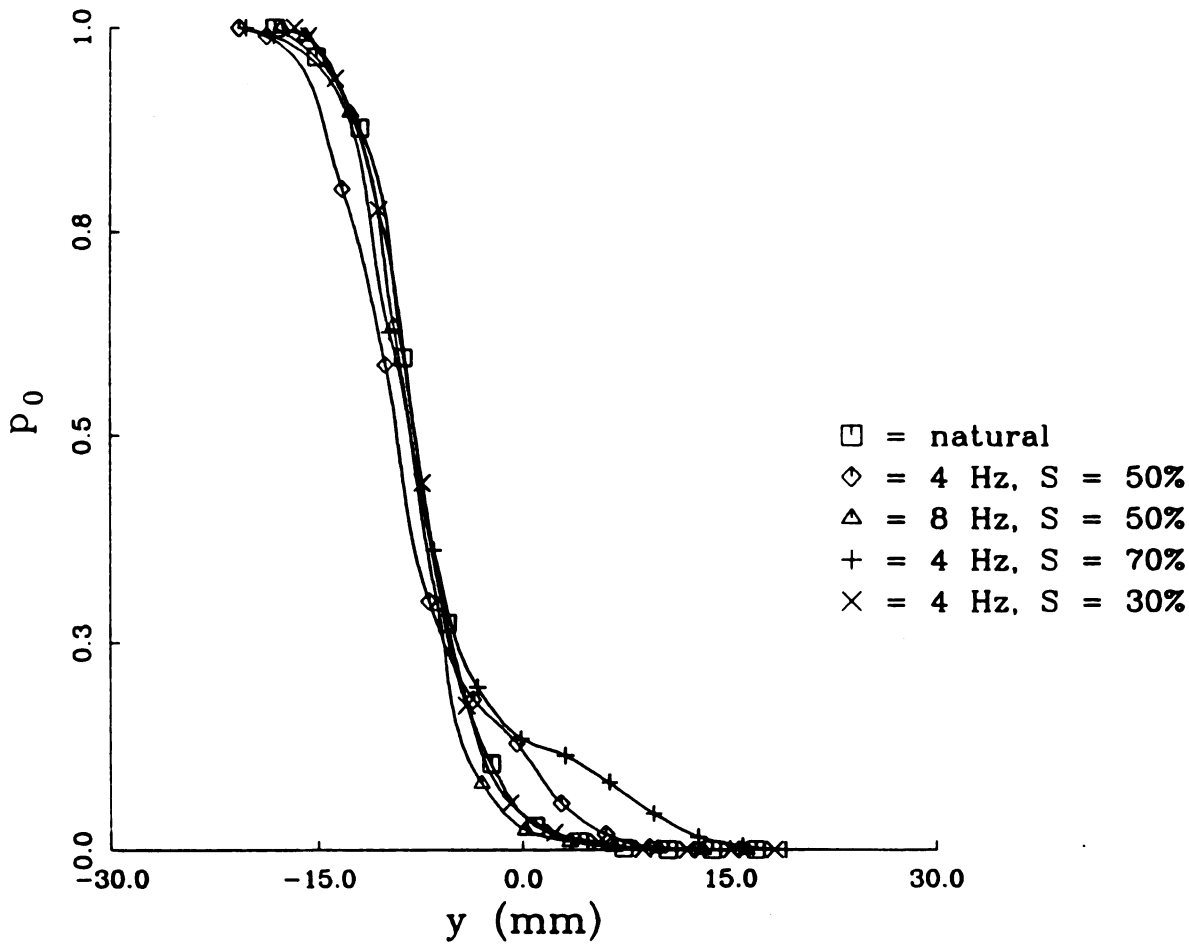

Figure 24. Transverse profiles of pure low-speed fluid probability.

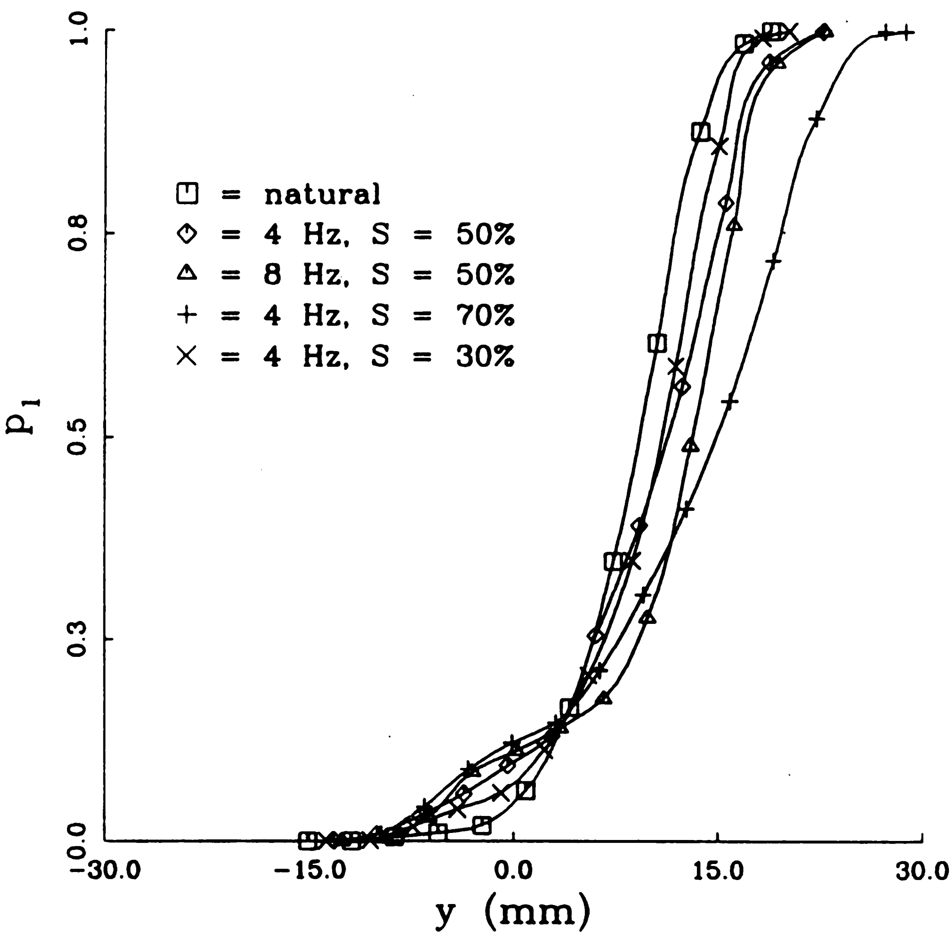

Figure 25. Transverse profiles of pure high-speed fluid probability.

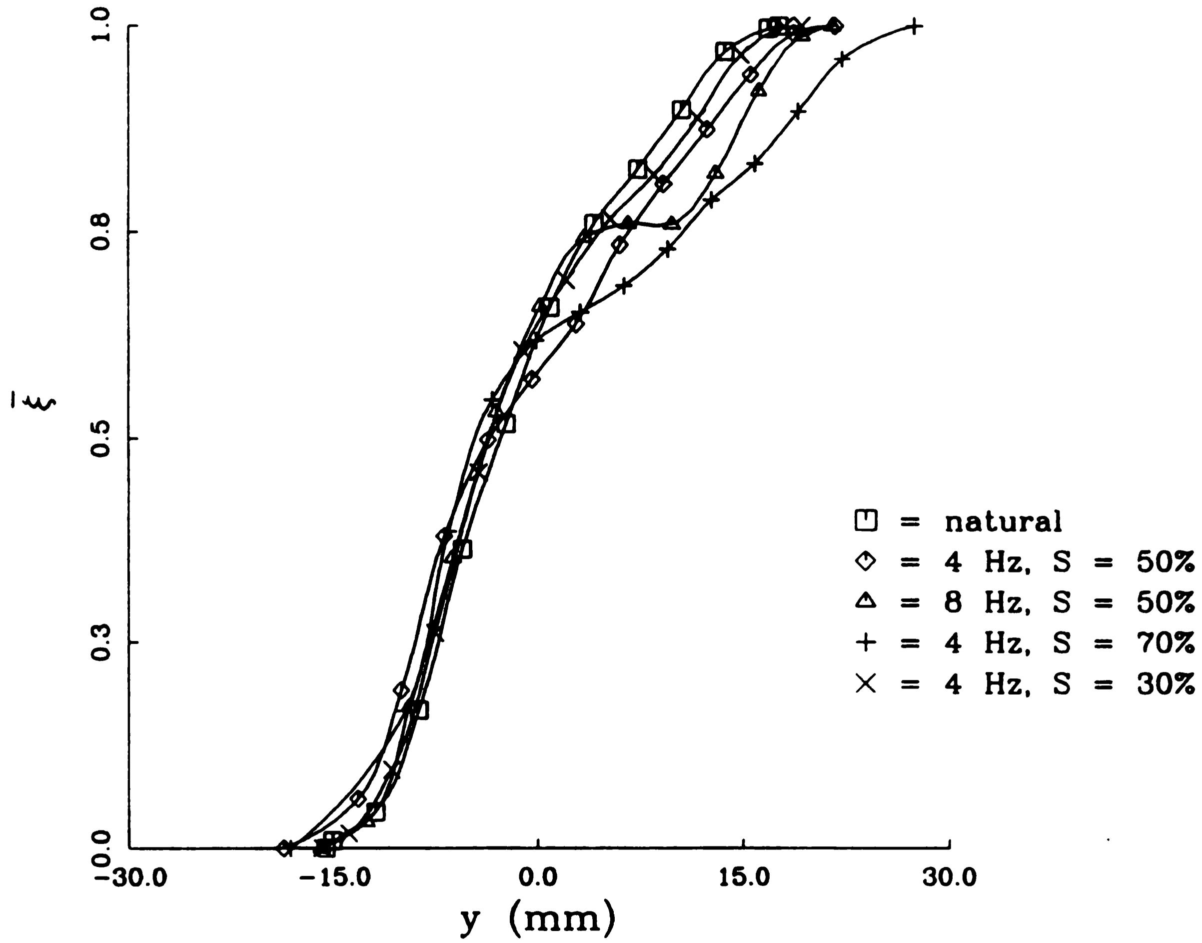

Figure 26. Transverse profiles of average high-speed fluid concentration.

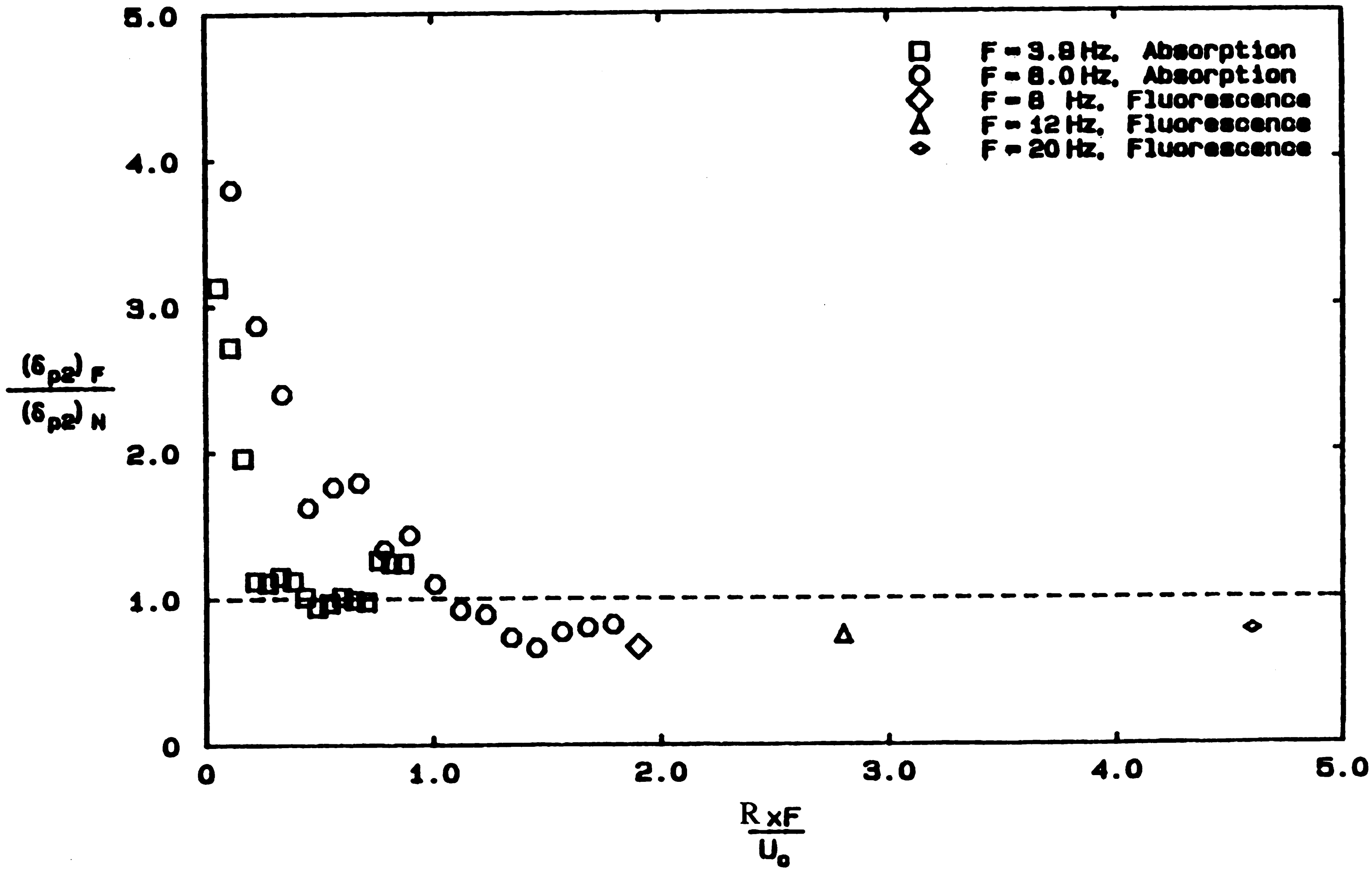

Figure 27. Ratio of forced product thickness to natural product thickness as a function of X_{WO} : high Reynolds number case (from Roberts (1985)).

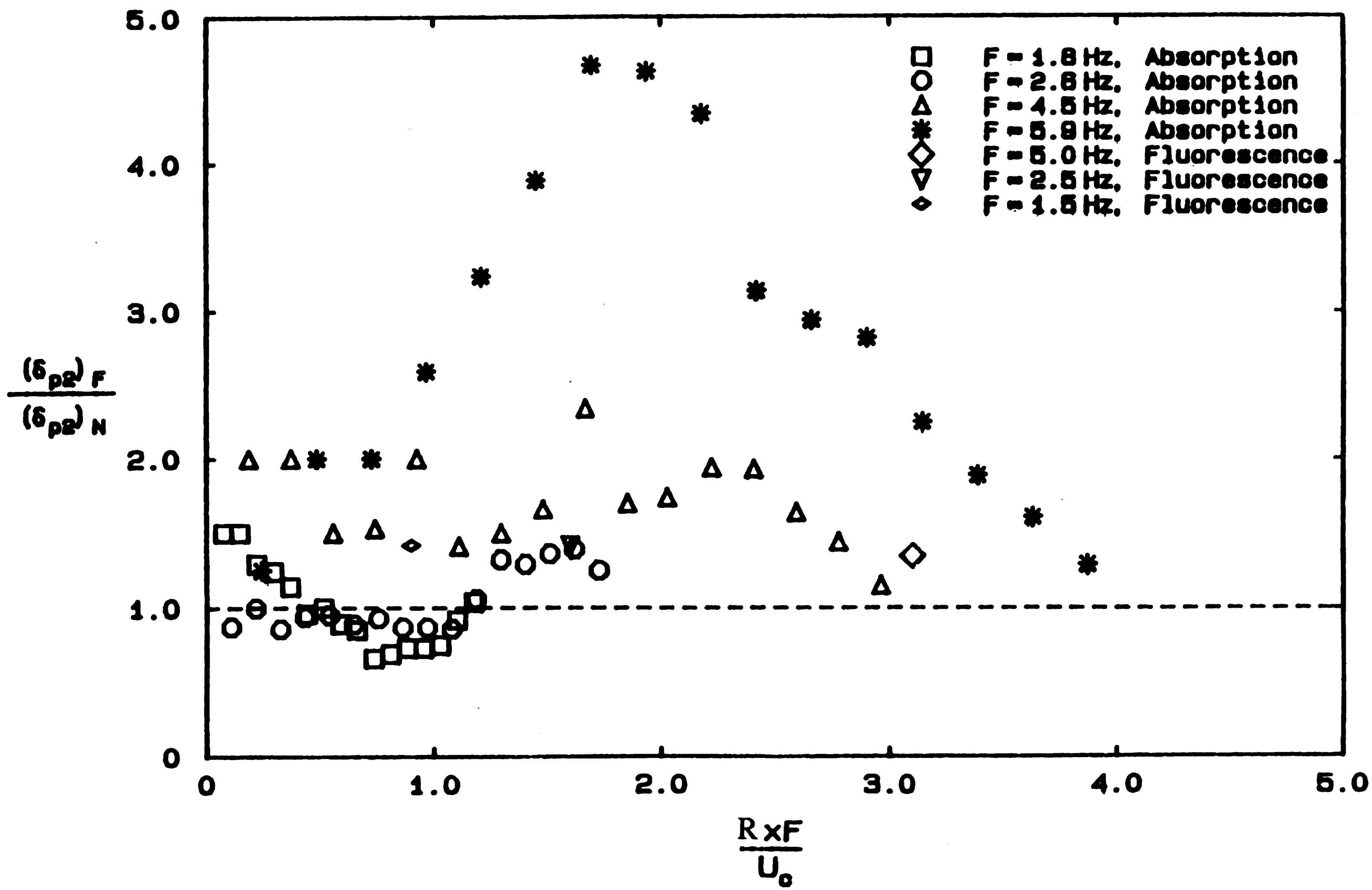

Figure 28. Ratio of forced product thickness to natural product thickness as a function of X_{WO} : low Reynolds number case (from Roberts (1985)).